REPORT DOCUMENTATION PAGE

Form Approved
OMB No. 0704-0188

1. REPORT DATE *(DD-MM-YYYY)*
February 2012

2. REPORT TYPE
Viewgraph

3. DATES COVERED *(From - To)*
February 2012- April 2012

4. TITLE AND SUBTITLE
Non-Reactive Shear-Coaxial Jets with and without Transverse Acoustic Forcing

5a. CONTRACT NUMBER
In-House

5b. GRANT NUMBER

5c. PROGRAM ELEMENT NUMBER

6. AUTHOR(S)
Sophonias Teshome

5d. PROJECT NUMBER

5e. TASK NUMBER

5f. WORK UNIT NUMBER
23080533

7. PERFORMING ORGANIZATION NAME(S) AND ADDRESS(ES)

Air Force Research Laboratory (AFMC)
AFRL/RQRC
10 E. Saturn Blvd.
Edwards AFB CA 93524-7680

8. PERFORMING ORGANIZATION REPORT NO.

9. SPONSORING / MONITORING AGENCY NAME(S) AND ADDRESS(ES)
Air Force Research Laboratory (AFMC)
AFRL/RQR
5 Pollux Drive
Edwards AFB CA 93524-7048

10. SPONSOR/MONITOR'S ACRONYM(S)

11. SPONSOR/MONITOR'S REPORT NUMBER(S)
AFRL-RZ-ED-VG-2012-125

12. DISTRIBUTION / AVAILABILITY STATEMENT
Distribution A: Approved for Public Release; Distribution Unlimited. PA#12271

13. SUPPLEMENTARY NOTES
Ph.D. Defense, UCLA, Los Angeles, CA
23 April 2012

14. ABSTRACT

This research has concentrated on the characterization of mixing for typical liquid rocket injectors. The conditions of interest have encompassed subcritical to supercritical pressures with temperatures below and above the critical temperature, with and without an acoustic field. The project has been largely experimental in-house. A single shear coaxial injector element has been thoroughly studied. This type of injector element is commonly used in many rocket engines (e.g., Space Shuttle Main Engine (SSME), Vulcain, RS-68, etc). It was found that the mixing in these injectors is governed primarily by the presence or absence of an acoustic field, the outer to inner jet area ratio and the inner jet lip thickness to inner jet diameter, the outer to inner momentum flux ratio, the reduced density of the inner jet, and on whether the pressure is subcritical and supercritical.

15. SUBJECT TERMS

16. SECURITY CLASSIFICATION OF:			17. LIMITATION OF ABSTRACT	18. NUMBER OF PAGES	19a. NAME OF RESPONSIBLE PERSON
					Doug Talley
a. REPORT	b. ABSTRACT	c. THIS PAGE	SAR	66	19b. TELEPHONE NO *(include area code)*
Unclassified	**Unclassified**	**Unclassified**			661-275-6174

Standard Form 298 (Rev. 8-98)
Prescribed by ANSI Std. 239.18

Non-Reactive Shear-Coaxial Jets with and without Transverse Acoustic Forcing

Sophonias Teshome

University of California, Los Angeles
Department of Mechanical and Aerospace Engineering

Ph.D. Thesis Defense
April 23, 2012

Motivation

- Feedback cycle between liquid rocket engine (LRE) combustion chamber pressure perturbations and unsteady combustion[1,2]
- Large amplitude fluctuations in pressure and combustion heat release rates ⇒ combustion instability

[1]Harrje, D.T., and Reardon, F.H.. *Scientific and Technical Information Office*, National Aeronautics and Space Administration, NASA SP-194, 1972.

[2]Schadow, K.C., Gutmark, E., Parr, T.P., Parr, D.M., Wilson, K.J., and Crump, J.H.. *19th AIAA Fluid Dynamics, Plasma Dynamics and Lasers Conference*, AIAA 1987-1326

Objective

- Impose external acoustic perturbations, and examine the response and stability characteristic of shear-coaxial injector flow to pressure perturbation

Acoustic/Pressure Perturbation → Shear-Coaxial Injector Flow

- Investigate influence of injector geometry on flow response to external pressure perturbation
- Vary the outer-to-inner jet momentum flux ratio, J, under subcritical chamber pressure condition, i.e., reduced pressure Pr = 0.44, 1.05

$$J = \frac{\rho_o u_o^2}{\rho_i u_i^2} \qquad Pr = \frac{P_{chamber}}{P_{critical,\mathrm{N}_2}} \qquad P_{critical,\mathrm{N}_2} = 3.4\,\mathrm{MPa}\ (493\,\mathrm{psi})$$

- Characterize mixing using dark-core length measurements
- Apply proper orthogonal decomposition of high-speed image pixel intensity fluctuations to extract spatial and temporal characteristics of prevalent coherent flow structures

Schematic of Experimental Facility

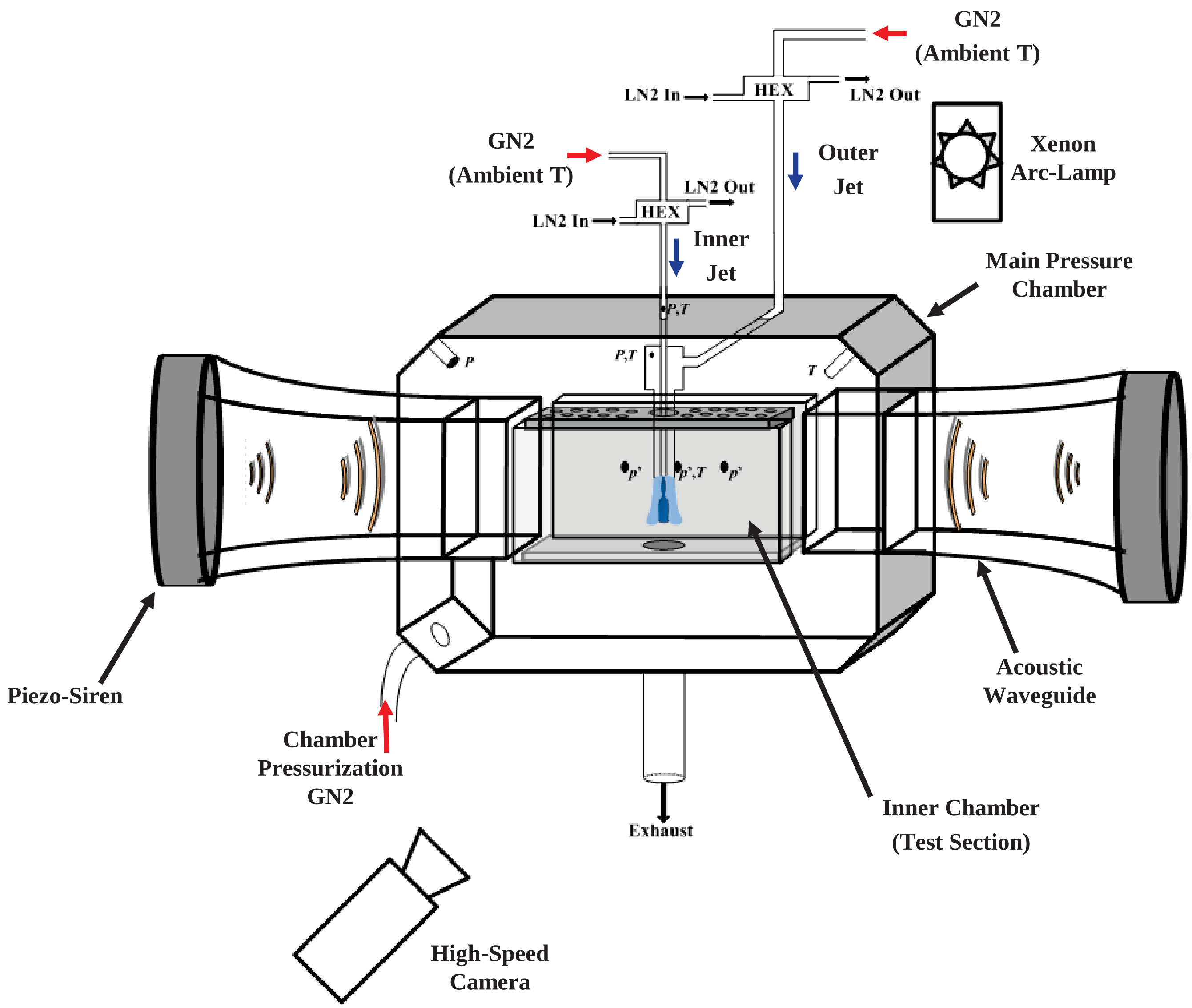

Image of Experimental Facility

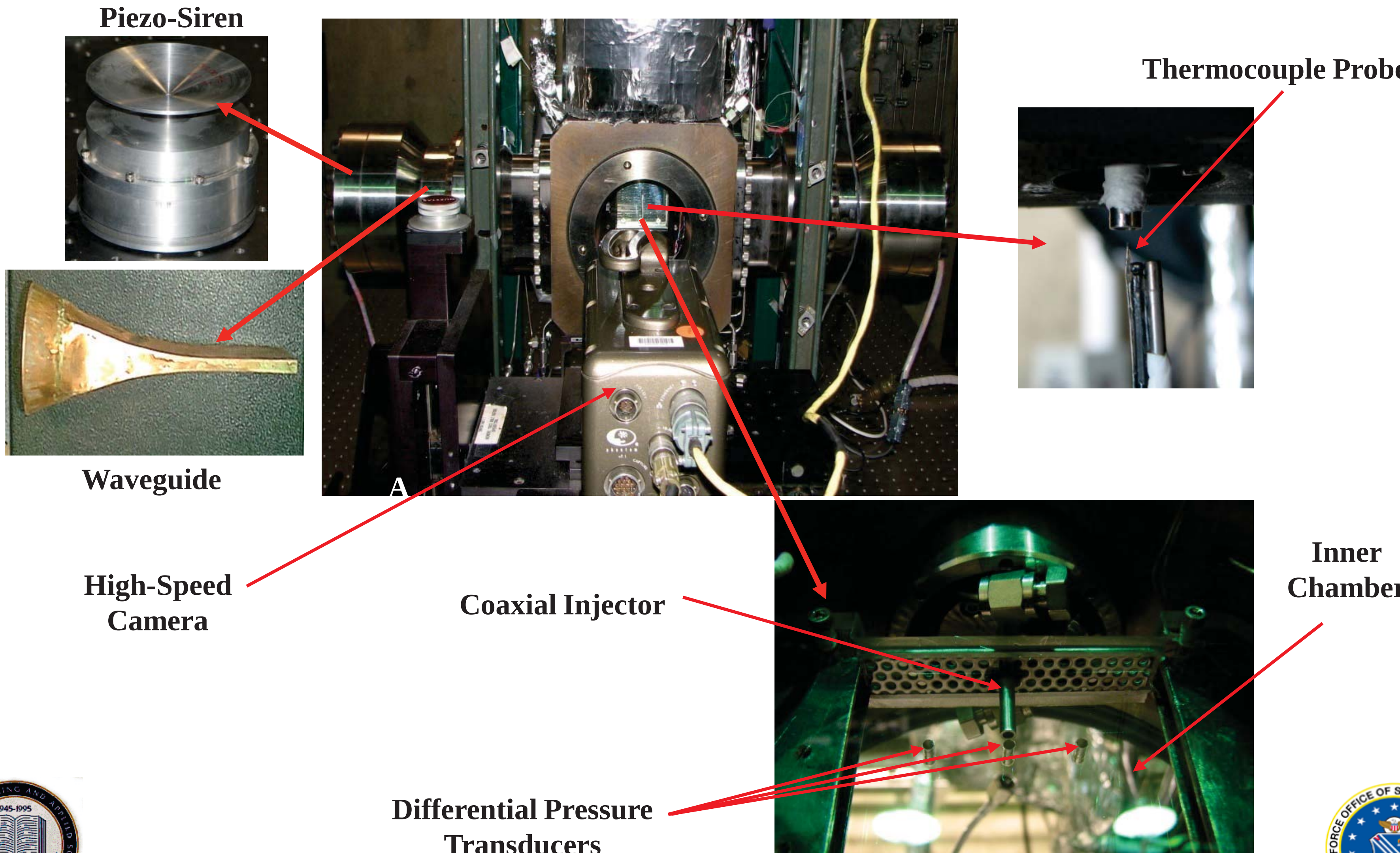

Distribution A: Approved for Public Release; Distribution Unlimited

Injector Assembly

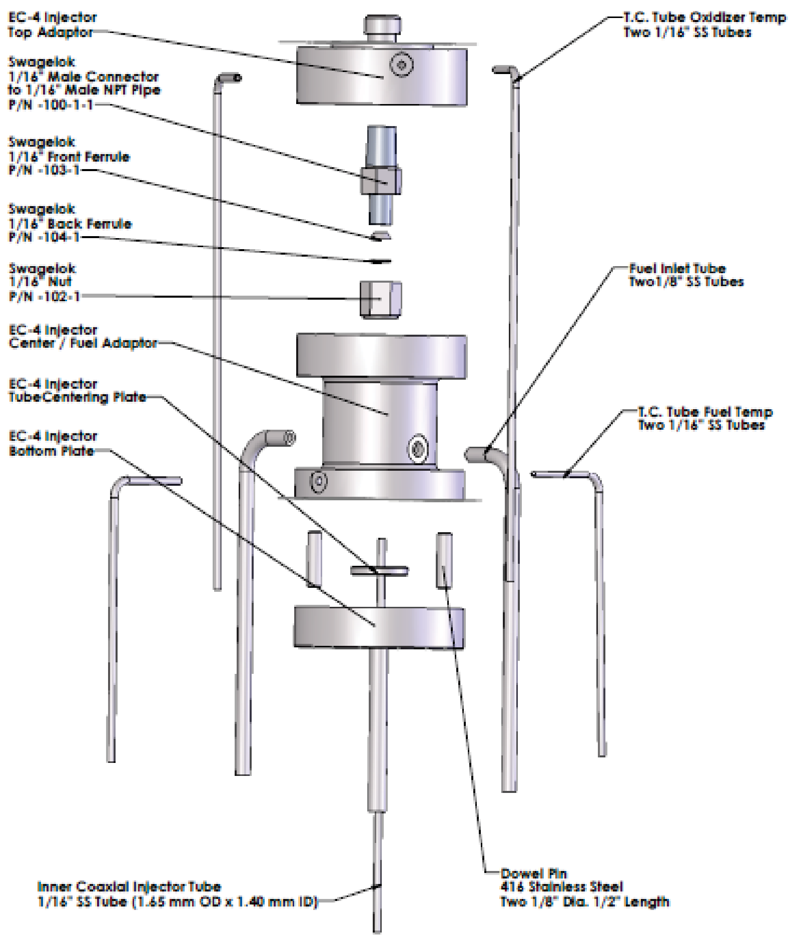

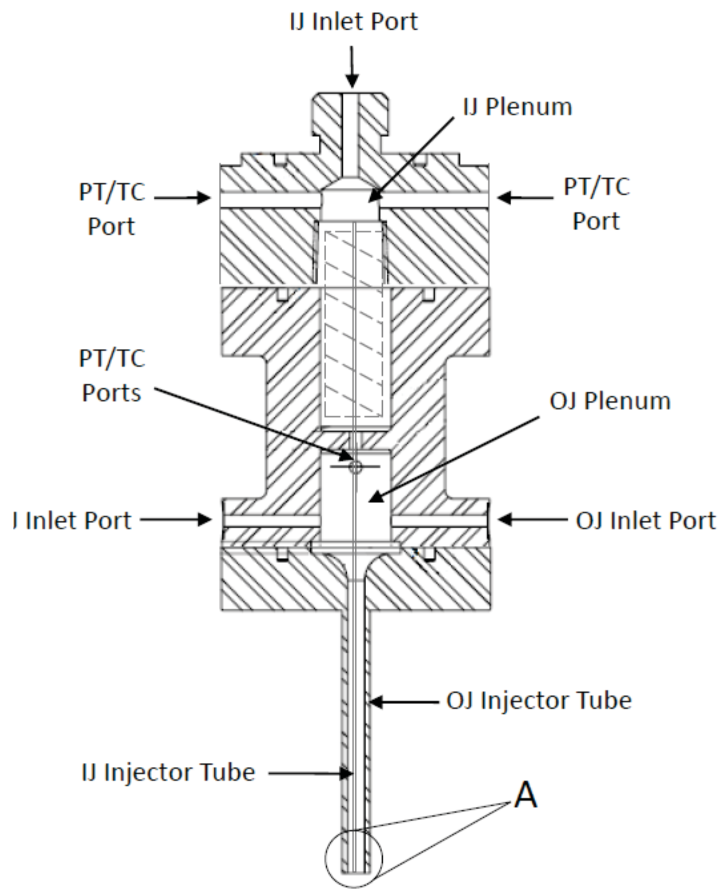

Injector Configuration

- Two types of outer-to-inner jet cross-sectional area ratios
  - Large Area Ratio, thin post (LAR-thin)
  - Small Area Ratio, thick post (SAR-thick)

A

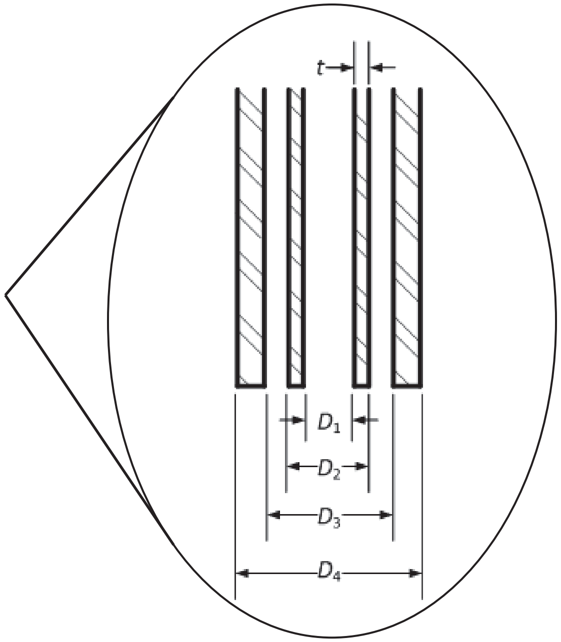

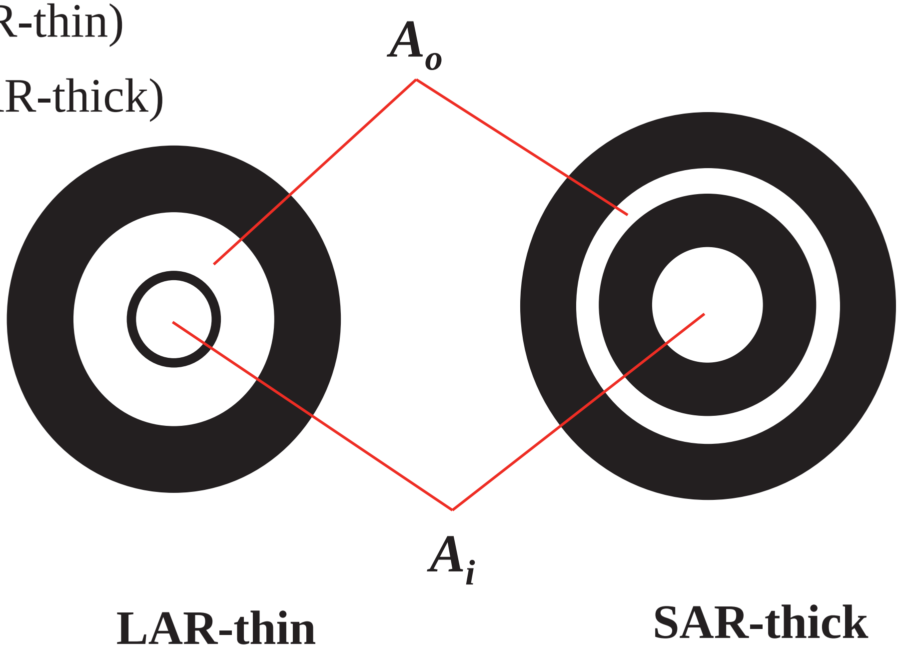

All dimensions in mm

Injector	D_1	D_2	D_3	D_4	t/D_1	A_o/A_i
LAR-thin	0.70	0.89	2.44	3.94	0.13	10.6
SAR-thick	1.47	3.96	4.70	6.35	0.84	2.90

Waveguides

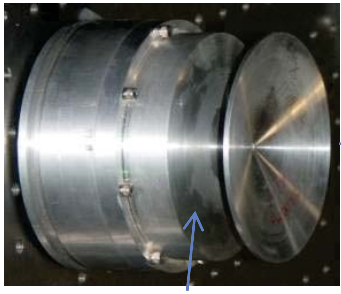

Acoustic Source – fits in circular end of waveguide

Circular end

Rectangular end – which connects to inner chamber

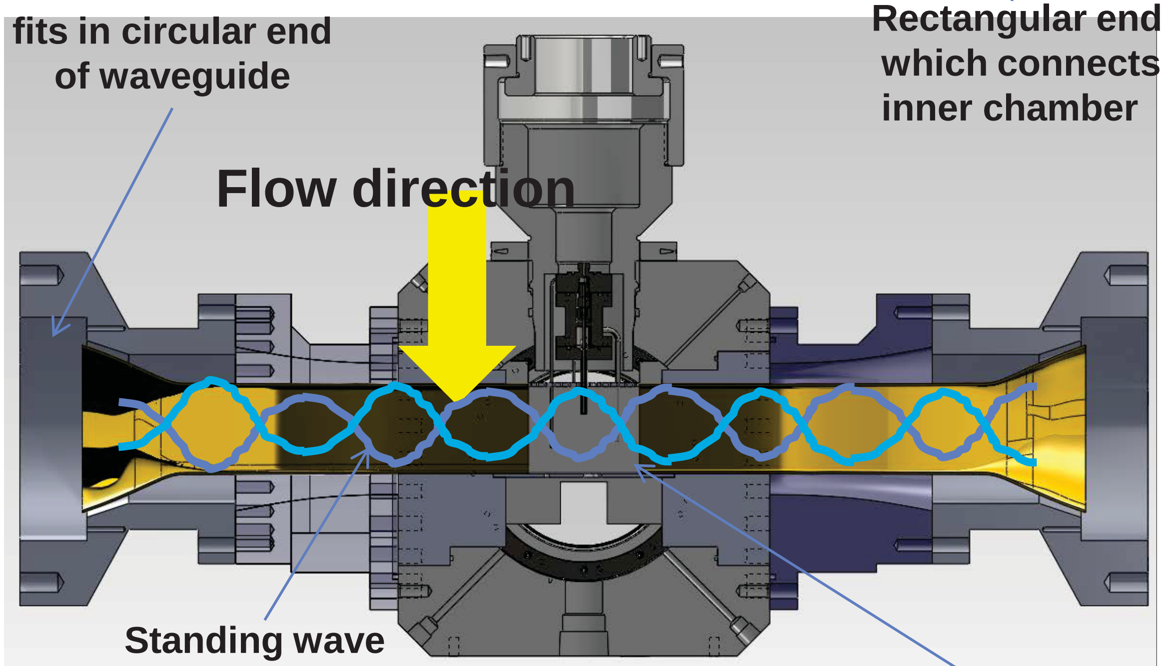

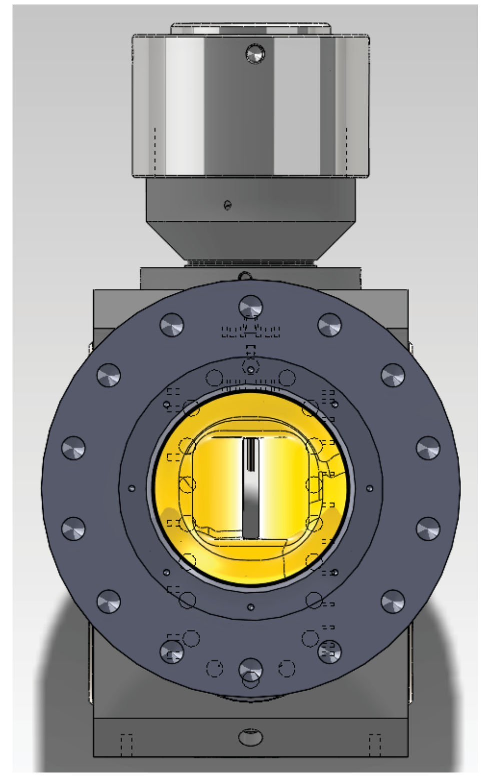

Standing wave (pressure anti-node case)

Waveguides viewed the front – cross section

Waveguide viewed from side (going from round to rectangular cross section)

Inner Chamber

Acoustic Field Set-Up: Pressure Antinode

- Pressure antinode (PAN) – condition of maximum pressure perturbation in the acoustic field
- Piezo-sirens forced in-phase
- Superposition of quasi-1D acoustic waves traveling in opposite directions ⇒ PAN at the jet location (geometric center of test section)

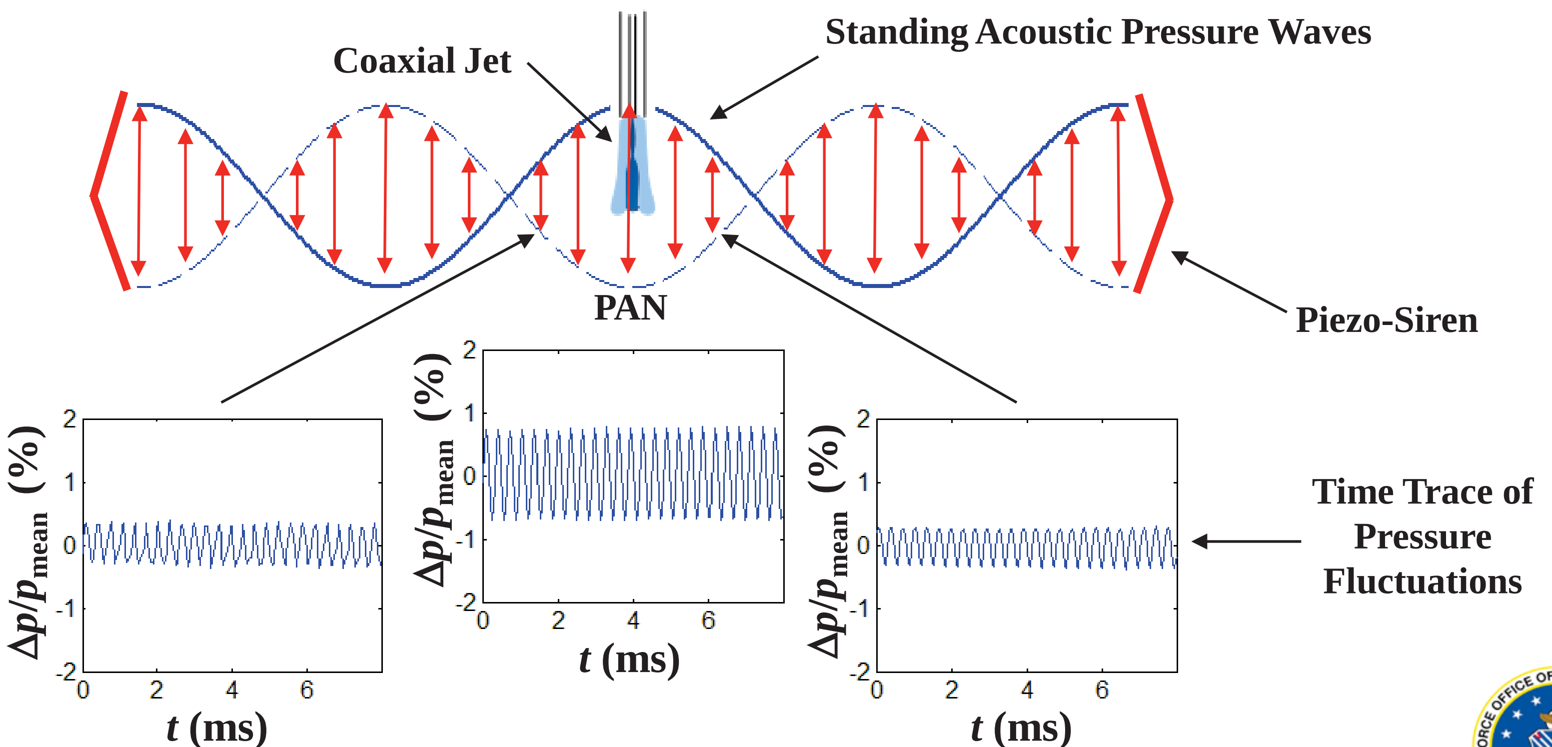

BASELINE FLOW
IMAGES AND DARK-CORE LENGTHS

Baseline Flows: LAR-thin Injector

$P_r = 0.44$

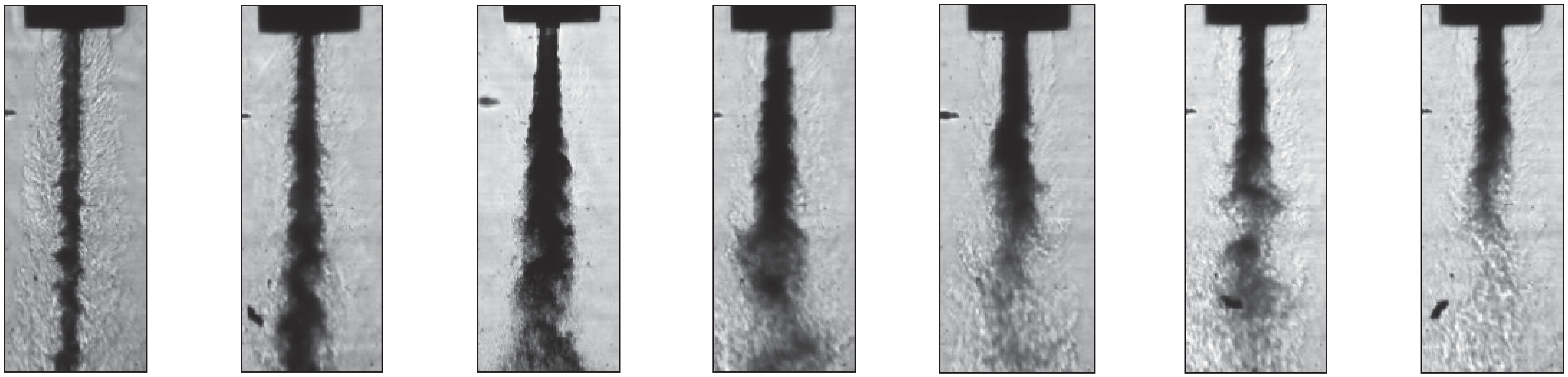

$J = 0.1$ 0.5 2.1 5.2 11 14 20

$P_r = 1.05$

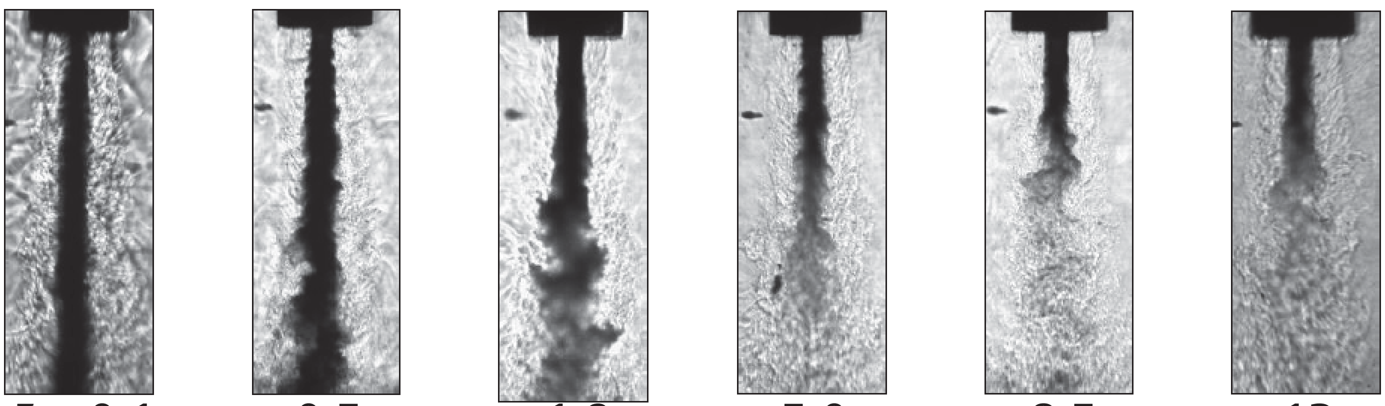

$J = 0.1$ 0.5 1.9 5.0 8.5 12

Baseline Flows: SAR-thick Injector

$P_r = 0.44$

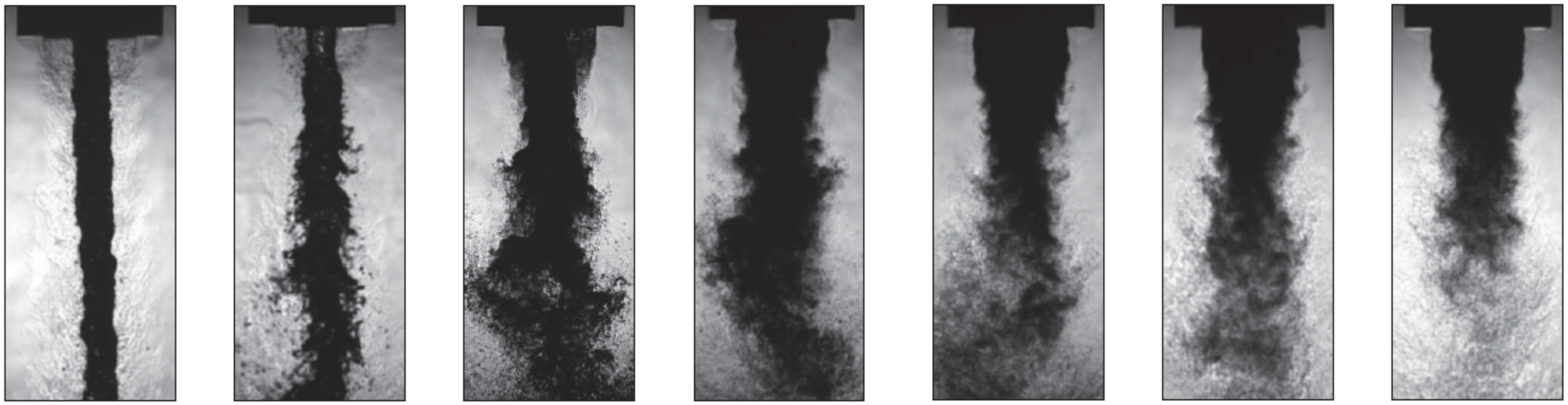

$J = 0.1$ 0.5 2.1 5.7 10 15 21

$P_r = 1.05$

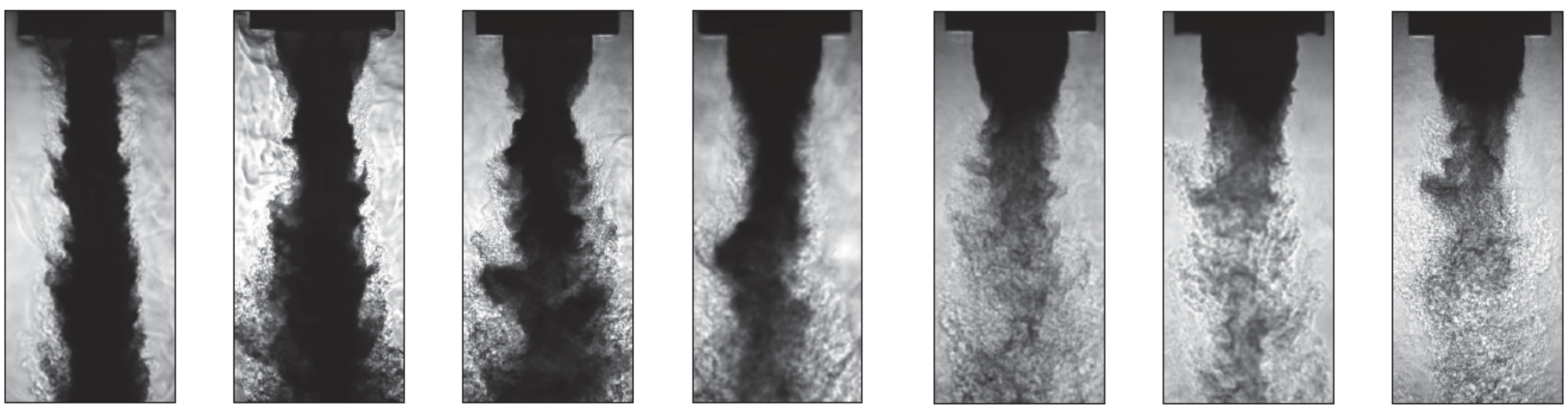

$J = 0.1$ 0.5 2.1 5.2 9.2 14 21

Dark-Core Length (DCL) Measurement

- First raw grayscale images were converted to binary images
- A contour was drawn around the "dark-column" in the binary image
- Axial length of the dark-column measured and defined as the Dark-Core Length, *L*

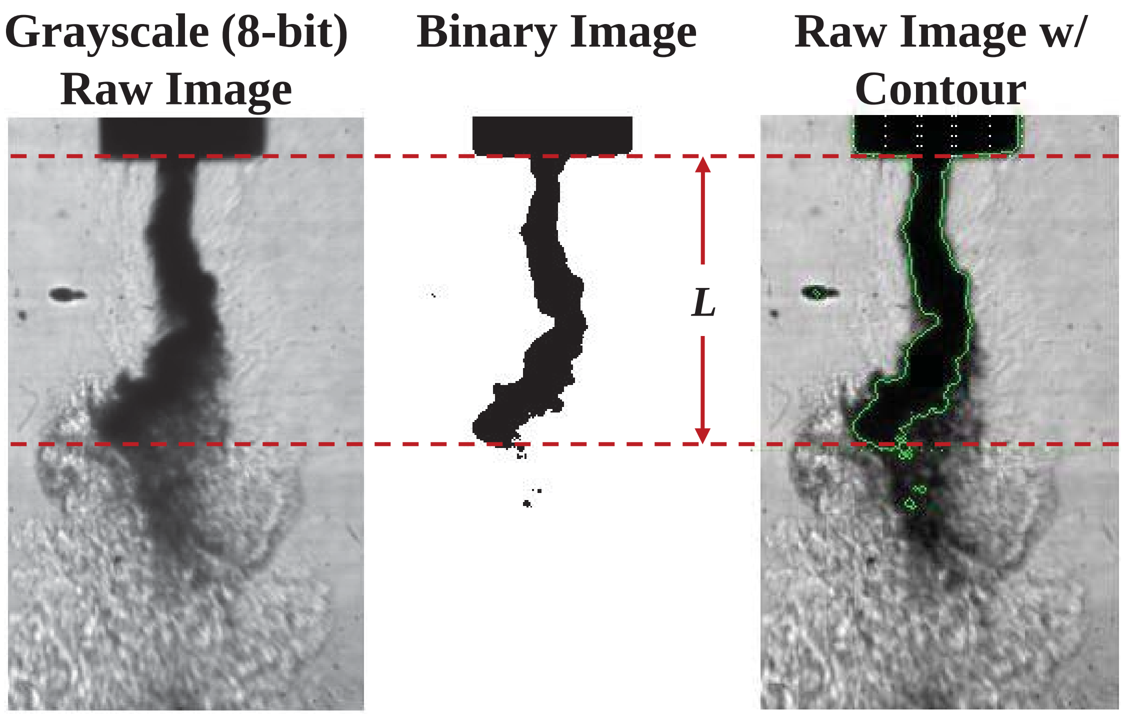

Baseline Normalized DCL, L_B/D_1

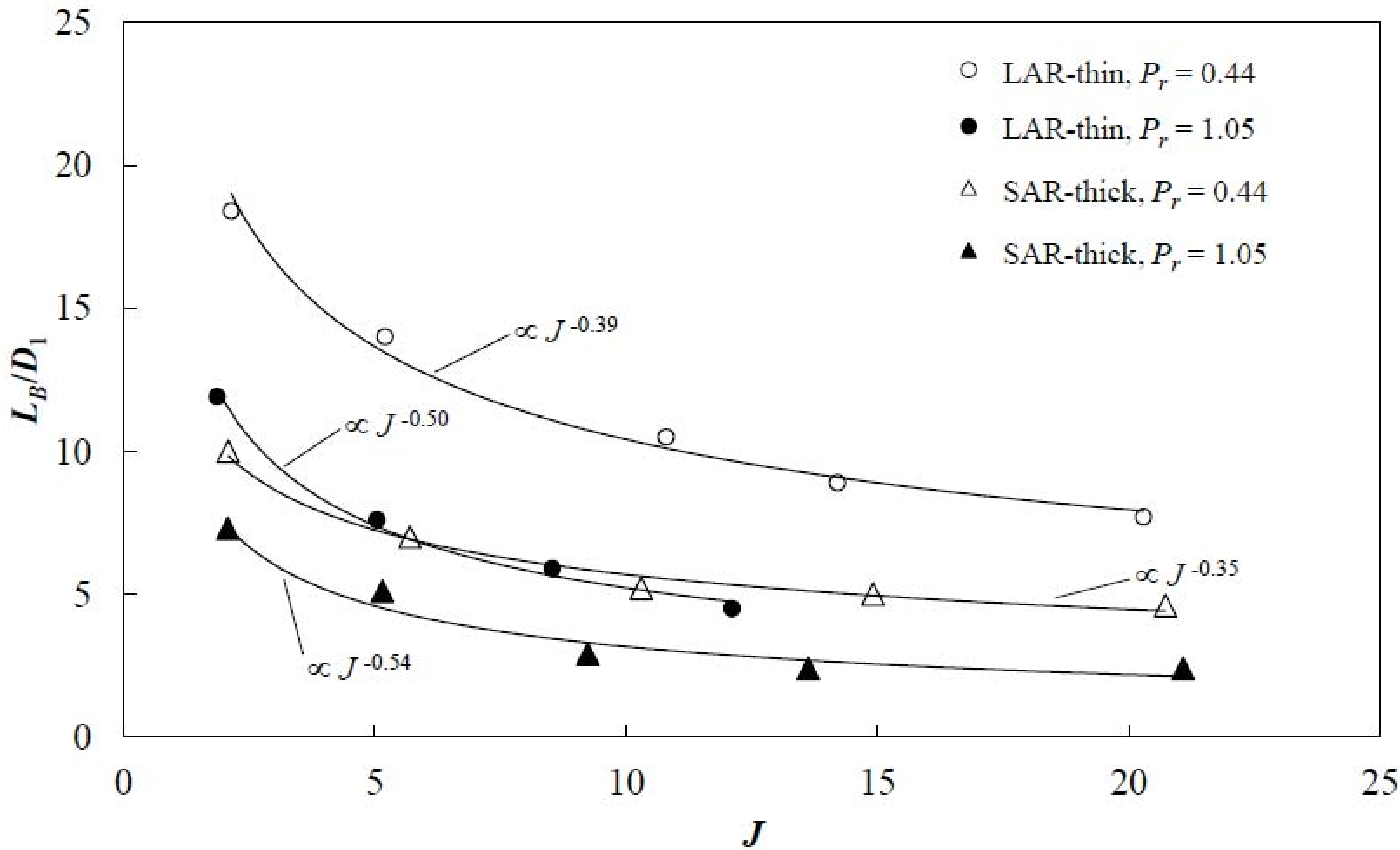

Geometric Configurations

LAR-thin

SAR-thin

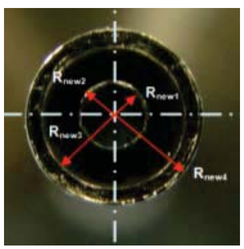

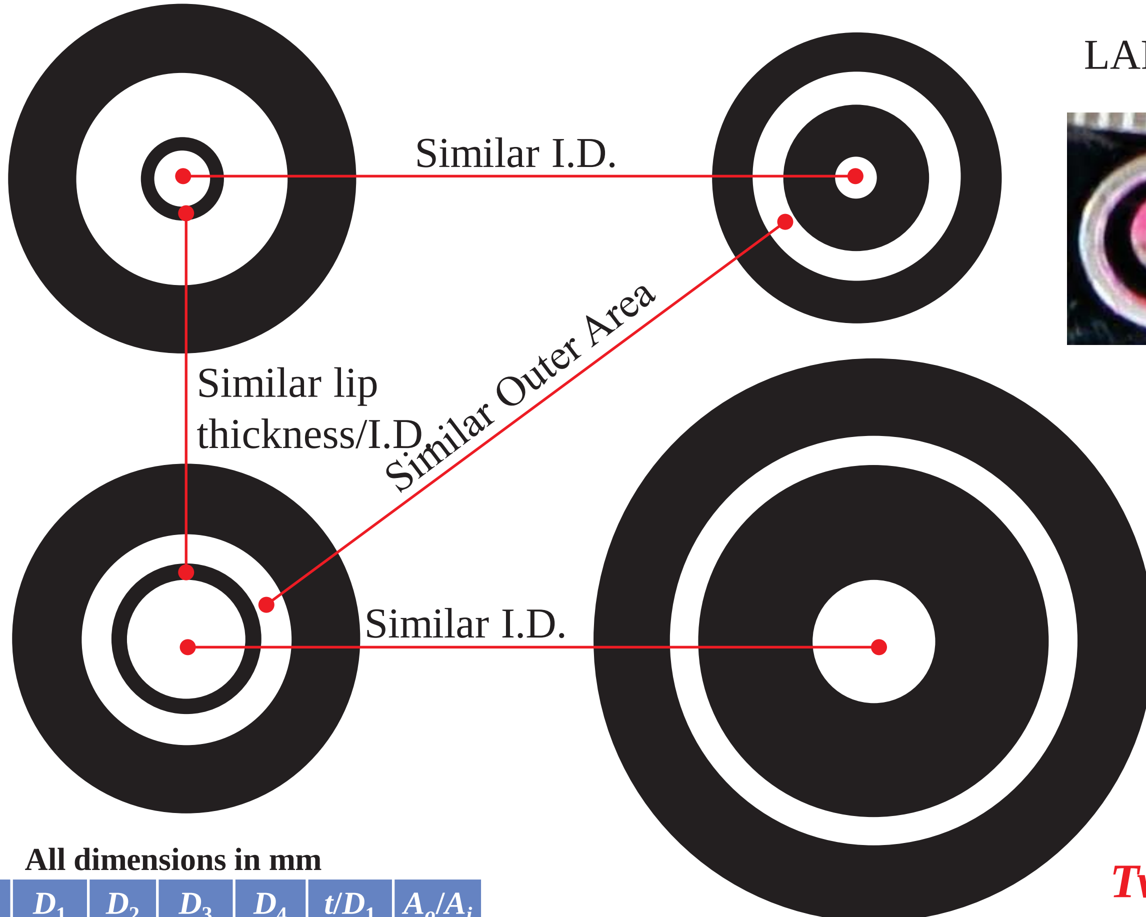

LAR-thick

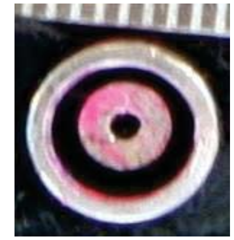

SAR-thick

Two recesses

All dimensions in mm

	D_1	D_2	D_3	D_4	t/D_1	A_o/A_i
LAR-thick	0.51	1.59	2.42	3.18	1.05	12.9
SAR-thin	1.40	1.65	2.44	3.94	0.09	1.6
SAR-thick	1.47	3.96	4.70	6.35	0.84	2.9
LAR-thin	0.70	0.89	2.44	3.94	0.13	10.6

SAR, LAR $\rightarrow$ Small, Large Area Ratio
Thick, Thin $\rightarrow$ Post lip thickness

Baseline Normalized DCL, L_B/D_1 – $P_r = 0.44$

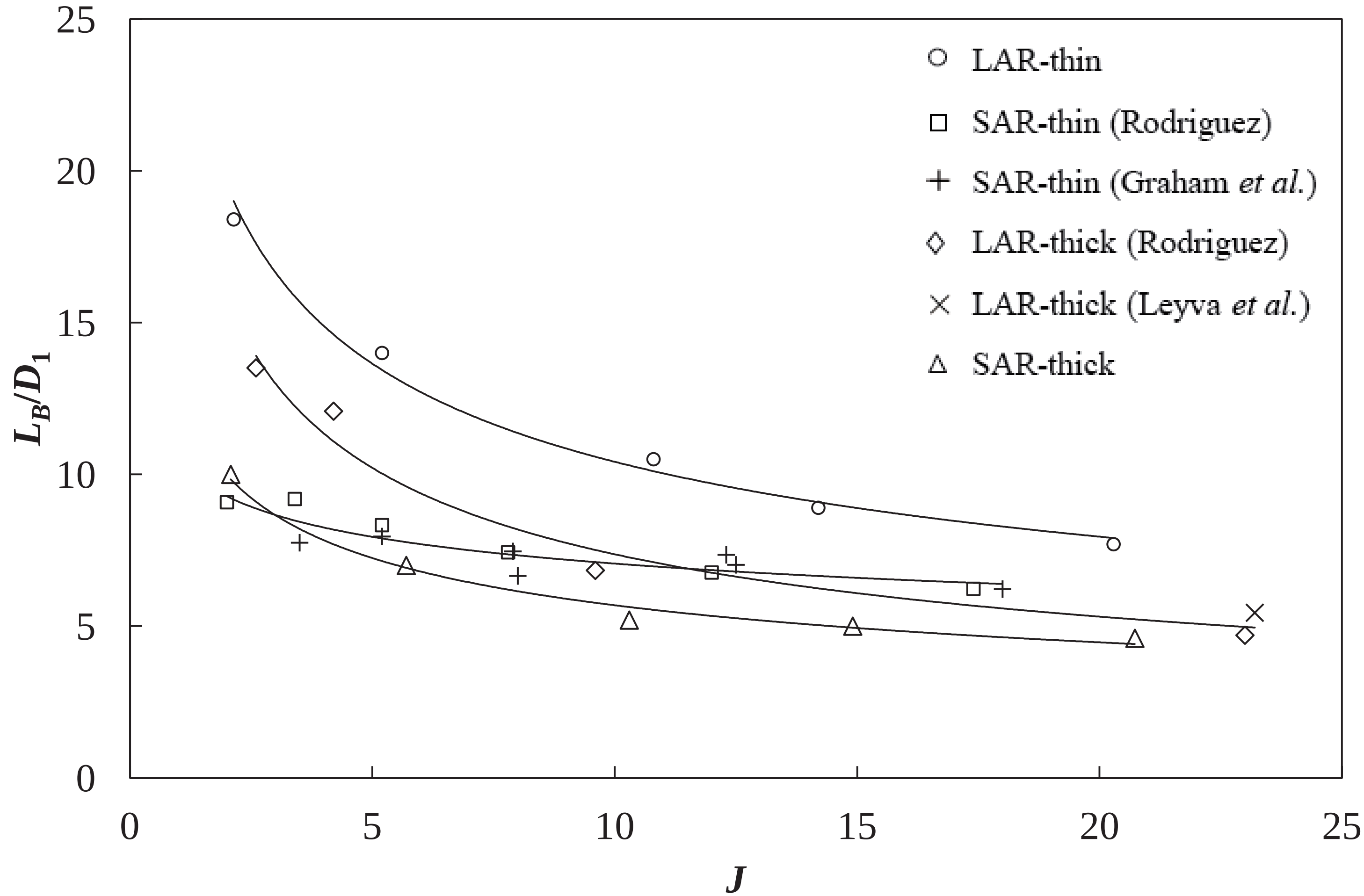

Baseline Normalized DCL, L_B/D_1 – $P_r = 1.05$

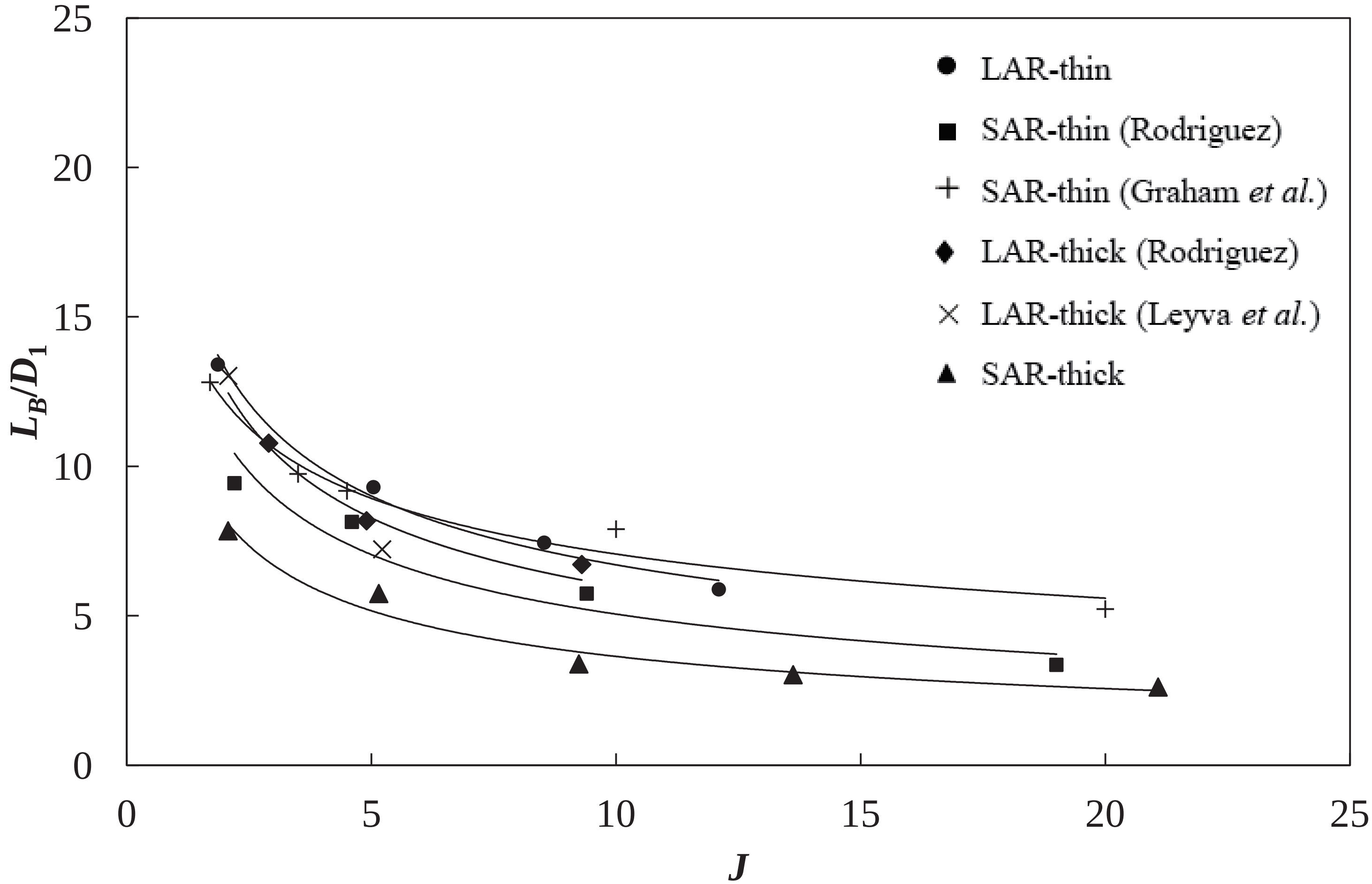

Baseline Normalized DCL, L_B/D_1 Collapse

$$\left(\frac{L_B}{D_1}\right) = c_1 J^{c_2} \left(\frac{t}{D_1}\right)^{c_3} \left(\frac{A_o}{A_i}\right)^{c_4}$$

P_r = 0.44

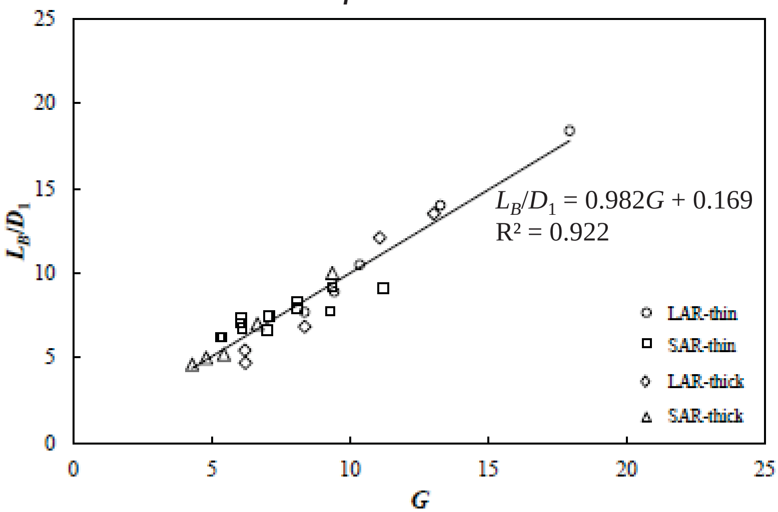

P_r = 1.05

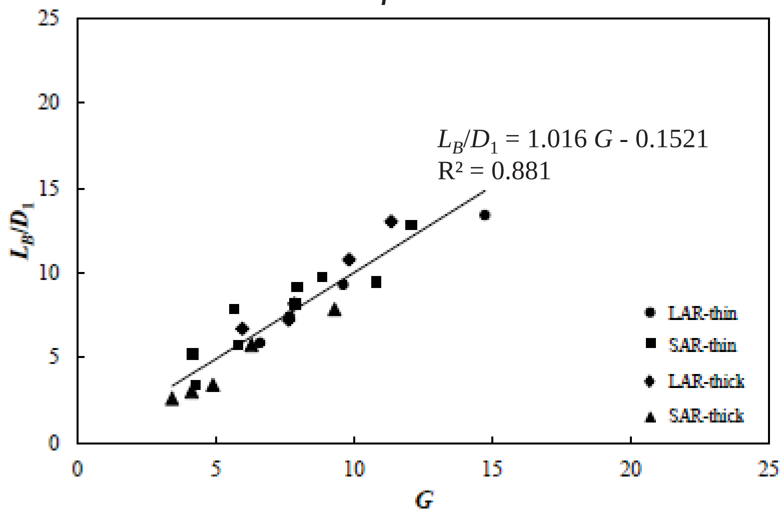

P_r	c_1	c_2	c_3	c_4
0.44	9	-0.34	-0.15	0.30
1.05	11	-0.43	-0.12	0.15

ACOUSTICALLY FORCED FLOW IMAGES AND DARK-CORE LENGTHS

Acoustically Forced Flows: LAR-thin – P_r = 0.44

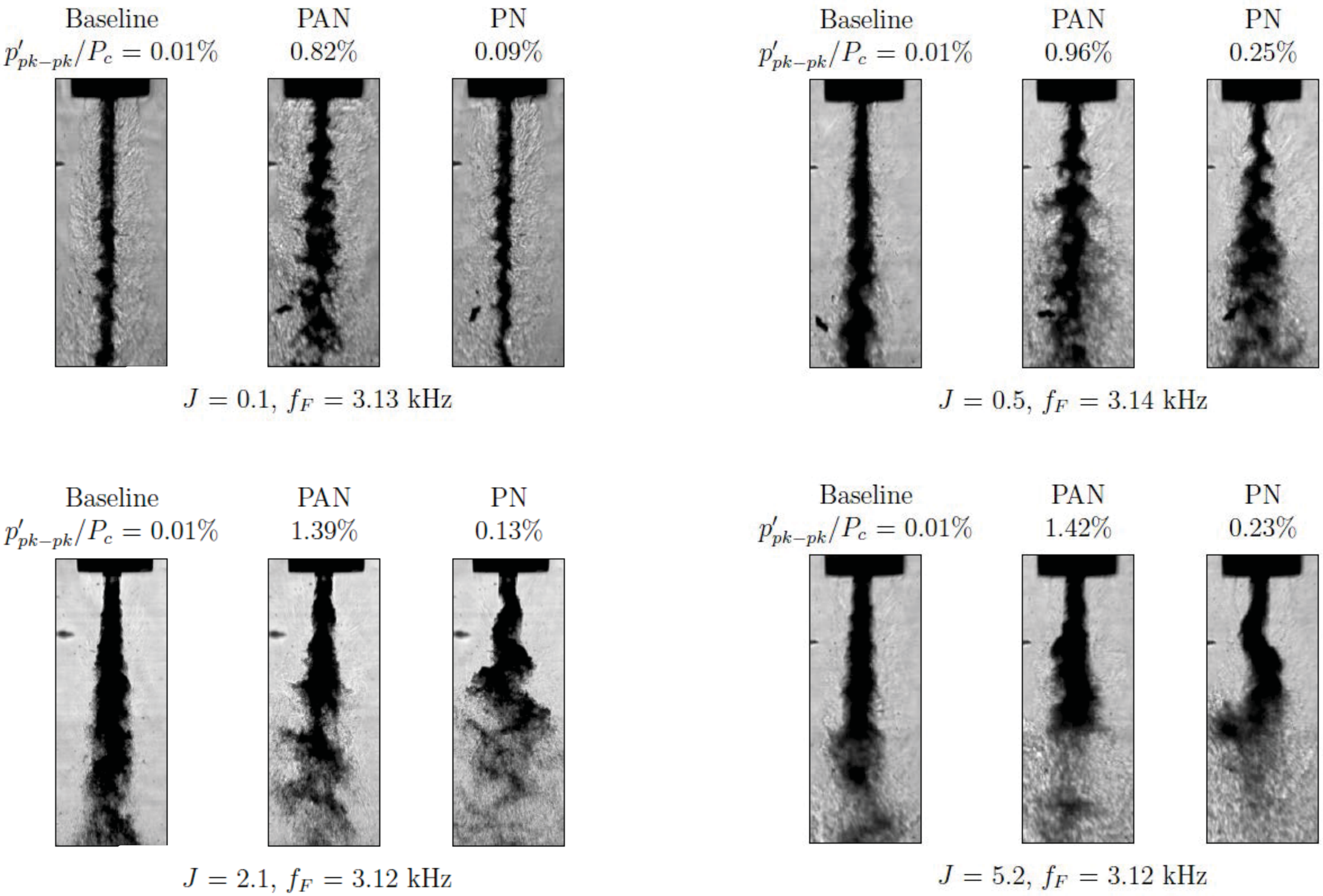

Acoustically Forced Flows: LAR-thin – P_r = 0.44

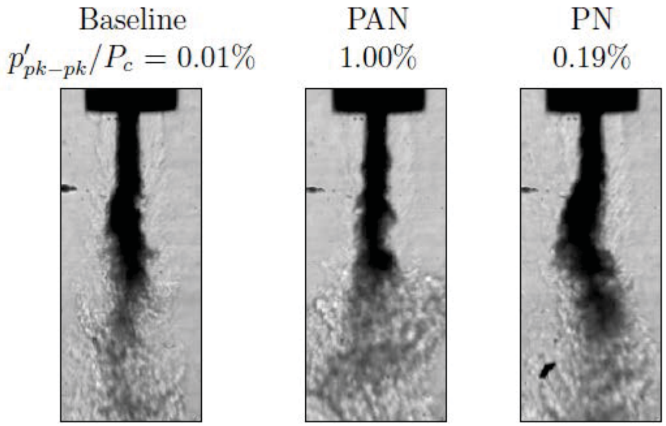

$J = 11,\ f_F = 3.10$ kHz

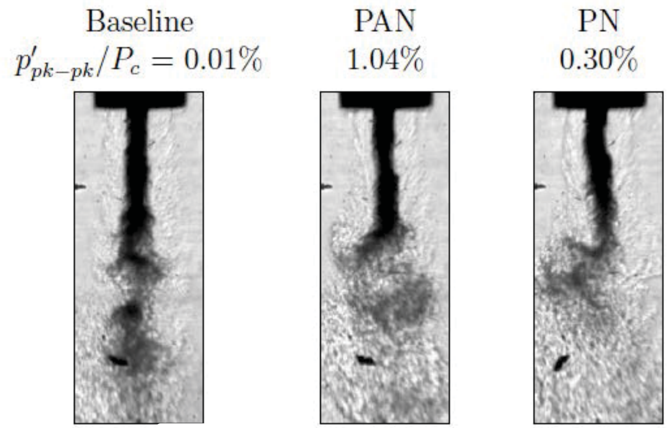

$J = 14,\ f_F = 3.11$ kHz

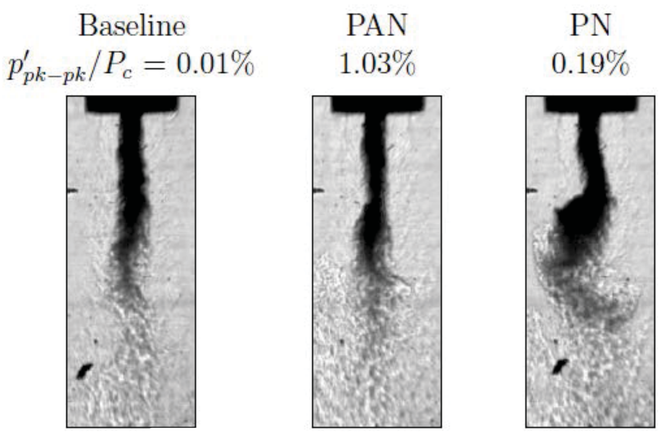

$J = 20,\ f_F = 3.11$ kHz

Acoustically Forced Flows: LAR-thin – P_r = 1.05

Baseline $p'_{pk-pk}/P_c = 0.01\%$ | PAN 0.77%

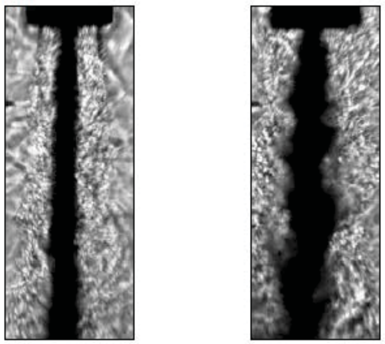

$J = 0.1,\ f_F = 3.16$ kHz

Baseline $p'_{pk-pk}/P_c = 0.00\%$ | PAN 0.98% | PN 0.11%

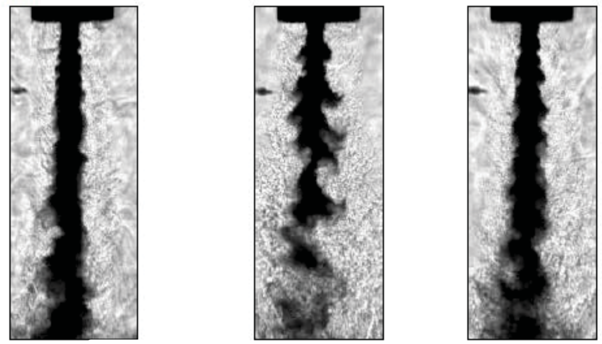

$J = 0.5,\ f_F = 3.10$ kHz

Baseline $p'_{pk-pk}/P_c = 0.01\%$ | PAN 0.75%

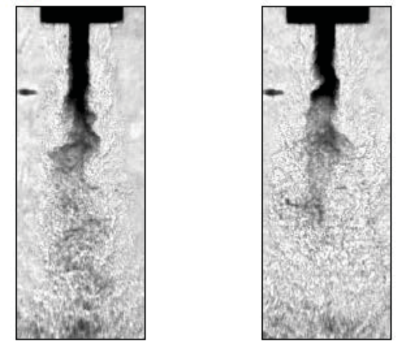

$J = 8.5,\ f_F = 3.10$ kHz

Baseline $p'_{pk-pk}/P_c = 0.01\%$ | PAN 1.22%

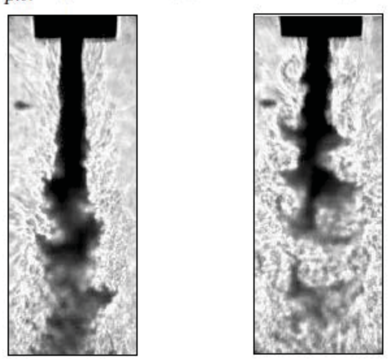

$J = 1.9,\ f_F = 3.10$ kHz

Baseline $p'_{pk-pk}/P_c = 0.01\%$ | PAN 0.54% | PN 0.05%

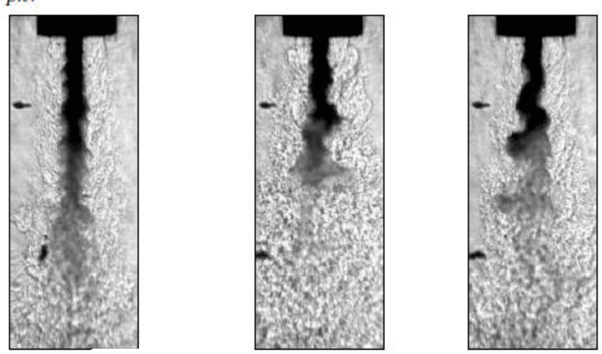

$J = 5.0,\ f_F = 3.41$ kHz

Baseline $p'_{pk-pk}/P_c = 0.01\%$ | PAN 1.02%

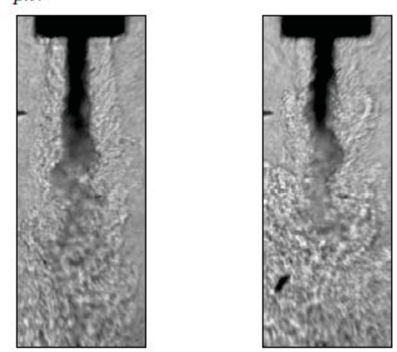

$J = 12,\ f_F = 3.10$ kHz

PAN Forcing: 40 μs Interval Image Sequence

LAR-thin, $P_r = 0.44$, $J = 0.5$

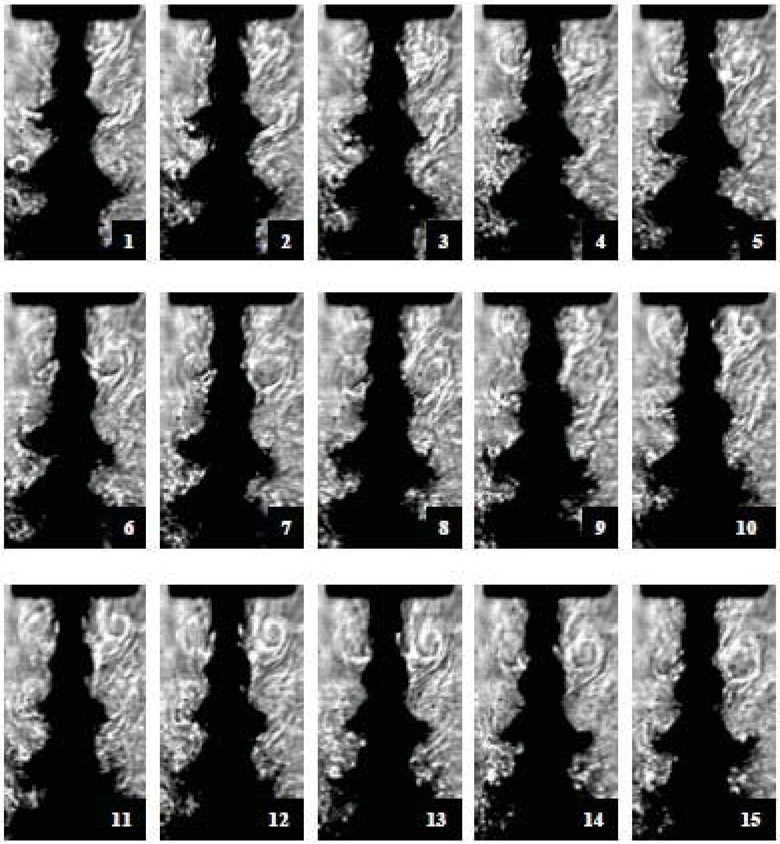

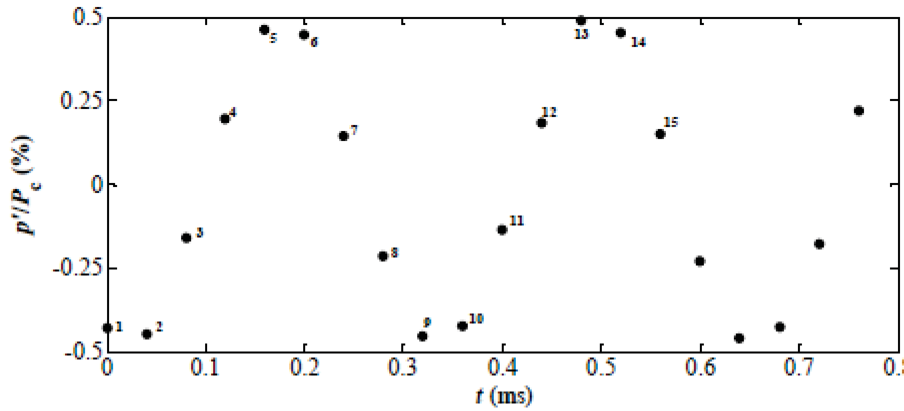

PAN Forcing: 40 μs Interval Image Sequence

LAR-thin, P_r = 0.44, J = 11

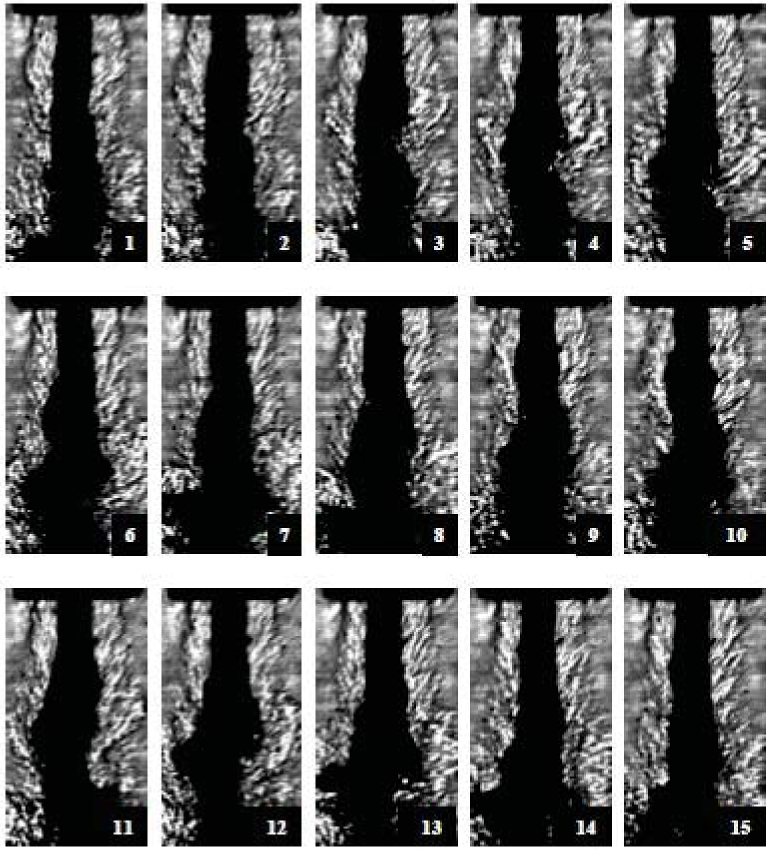

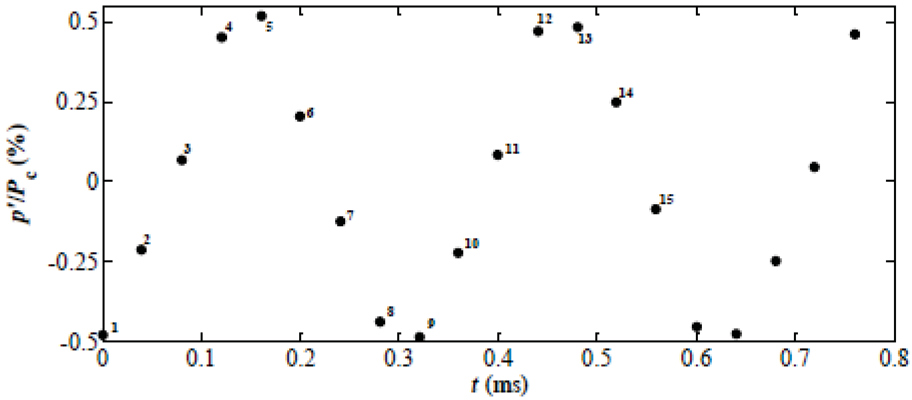

Acoustically Forced Flows: SAR-thick – P_r = 0.44

Baseline $p'_{pk-pk}/P_c = 0.02\%$ | PAN 1.32% | PN 0.21%

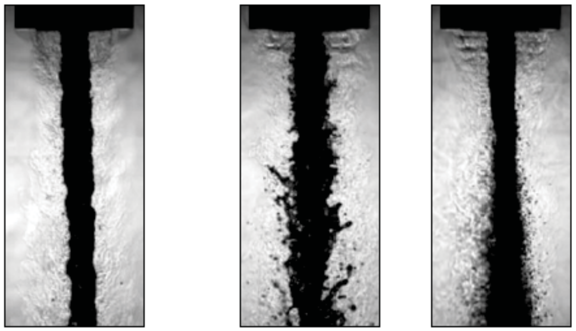

$J = 0.1,\ f_F = 3.10$ kHz

Baseline $p'_{pk-pk}/P_c = 0.02\%$ | PAN 1.27% | PN 0.19%

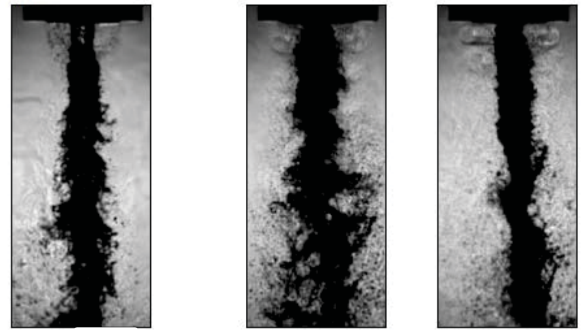

$J = 0.5,\ f_F = 3.04$ kHz

Baseline $p'_{pk-pk}/P_c = 0.02\%$ | PAN 1.42% | PN 0.28%

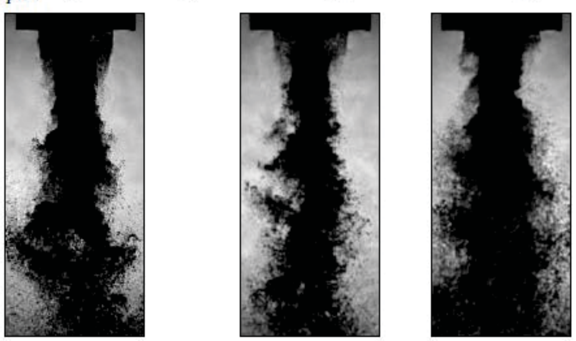

$J = 2.1,\ f_F = 3.07$ kHz

Baseline $p'_{pk-pk}/P_c = 0.02\%$ | PAN 1.06% | PN 0.14%

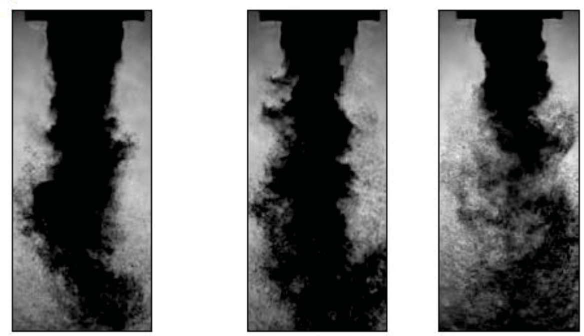

$J = 5.7,\ f_F = 3.11$ kHz

Acoustically Forced Flows: SAR-thick – P_r = 0.44

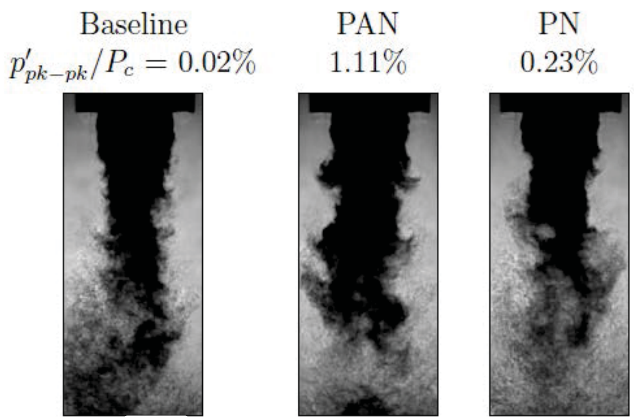

$J = 10,\ f_F = 3.11$ kHz

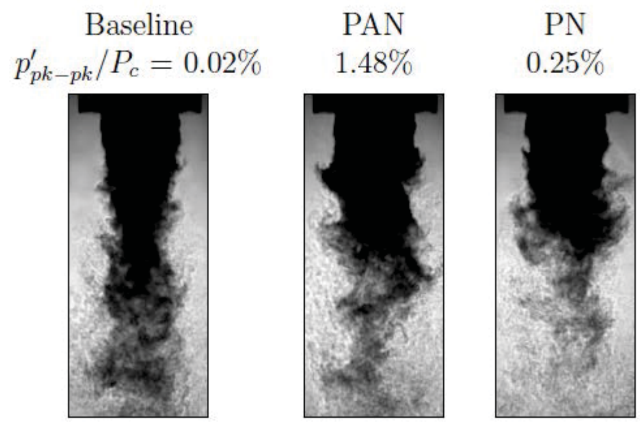

$J = 15,\ f_F = 3.04$ kHz

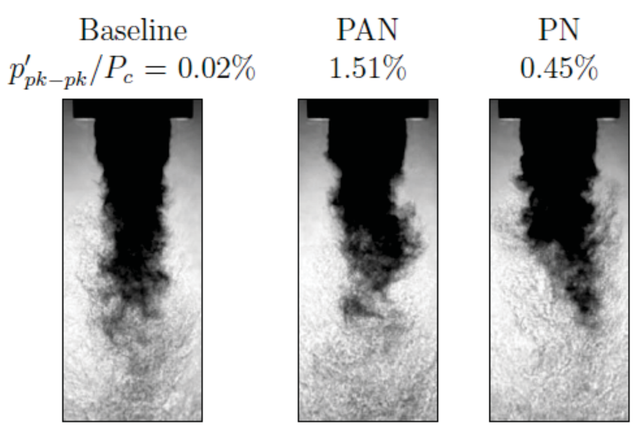

$J = 21,\ f_F = 3.11$ kHz

Acoustically Forced Flows: SAR-thick – $P_r = 1.05$

Baseline $p'_{pk-pk}/P_c = 0.01\%$ | PAN 0.69% | PN 0.13%

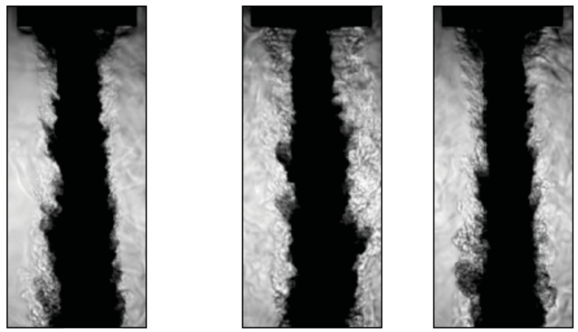

$J = 0.1,\ f_F = 3.12$ kHz

Baseline $p'_{pk-pk}/P_c = 0.01\%$ | PAN 0.67% | PN 0.40%

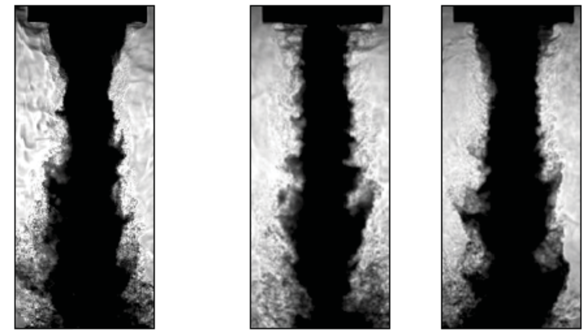

$J = 0.5,\ f_F = 3.00$ kHz

Baseline $p'_{pk-pk}/P_c = 0.01\%$ | PAN 1.17% | PN 0.23%

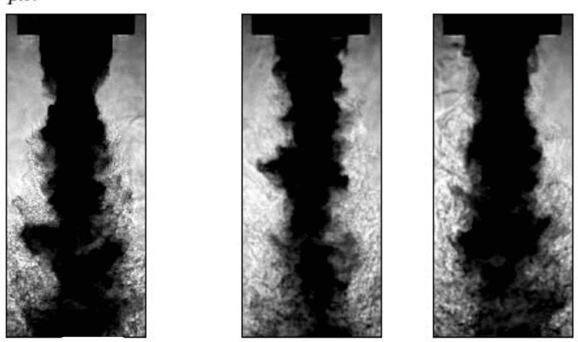

$J = 2.1,\ f_F = 3.04$ kHz

Baseline $p'_{pk-pk}/P_c = 0.01\%$ | PAN 0.93% | PN 0.14%

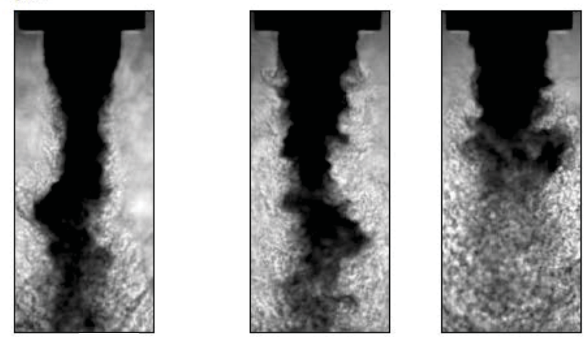

$J = 5.2,\ f_F = 3.08$ kHz

Acoustically Forced Flows: SAR-thick – $P_r = 1.05$

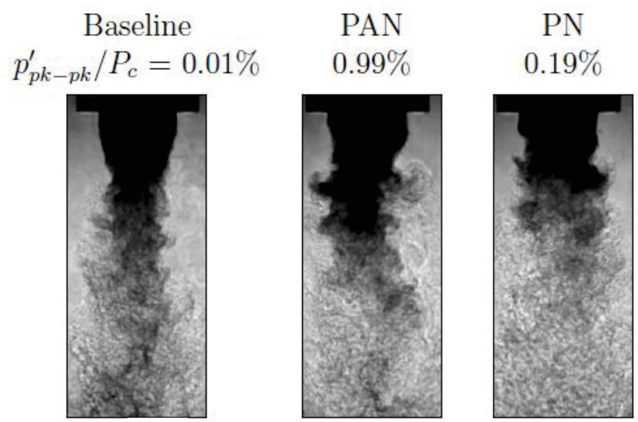

$J = 9.2,\ f_F = 3.11$ kHz

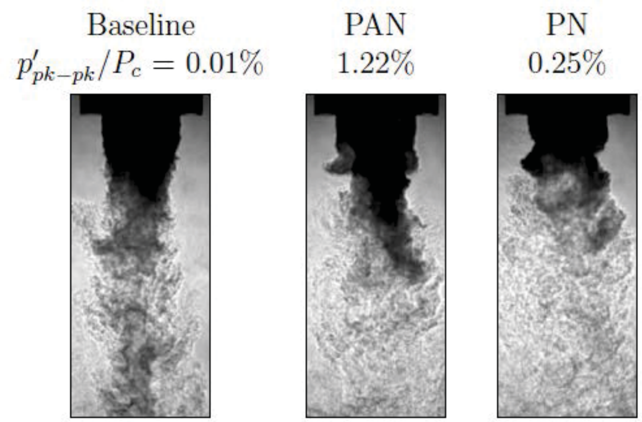

$J = 14,\ f_F = 3.04$ kHz

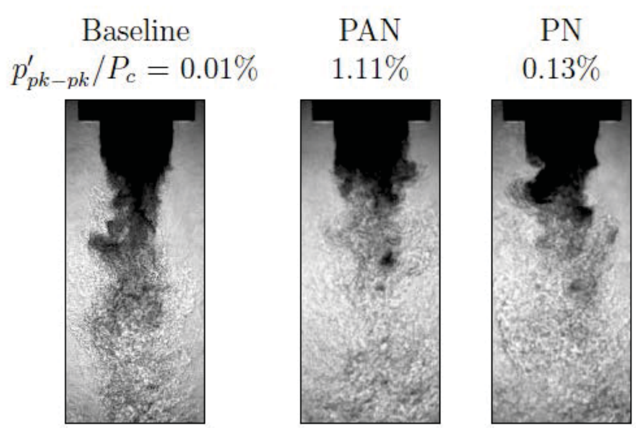

$J = 21,\ f_F = 3.12$ kHz

PAN Forcing: Normalized DCL, L_{PAN}/L_B

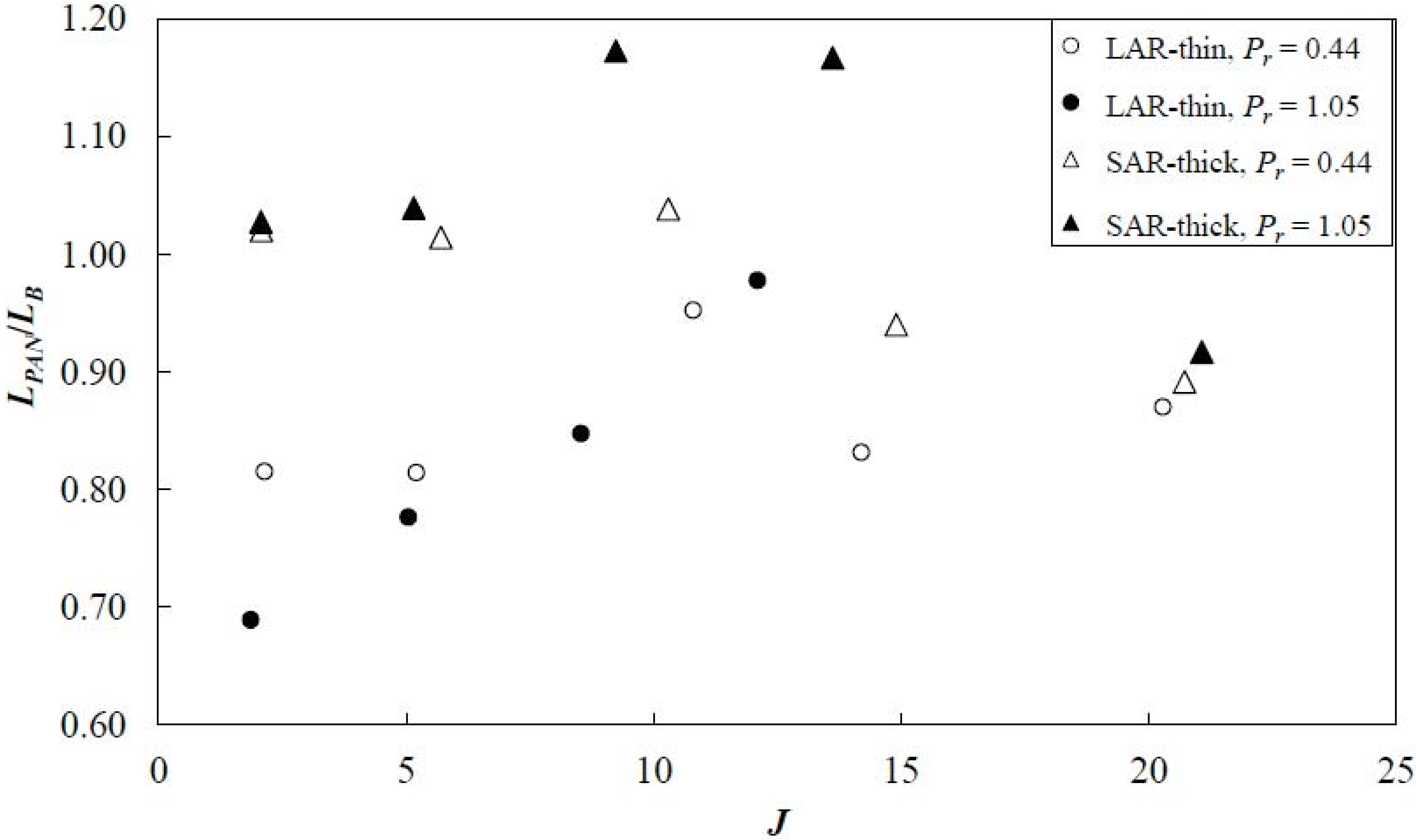

PN Forcing: Normalized DCL, L_{PN}/L_B

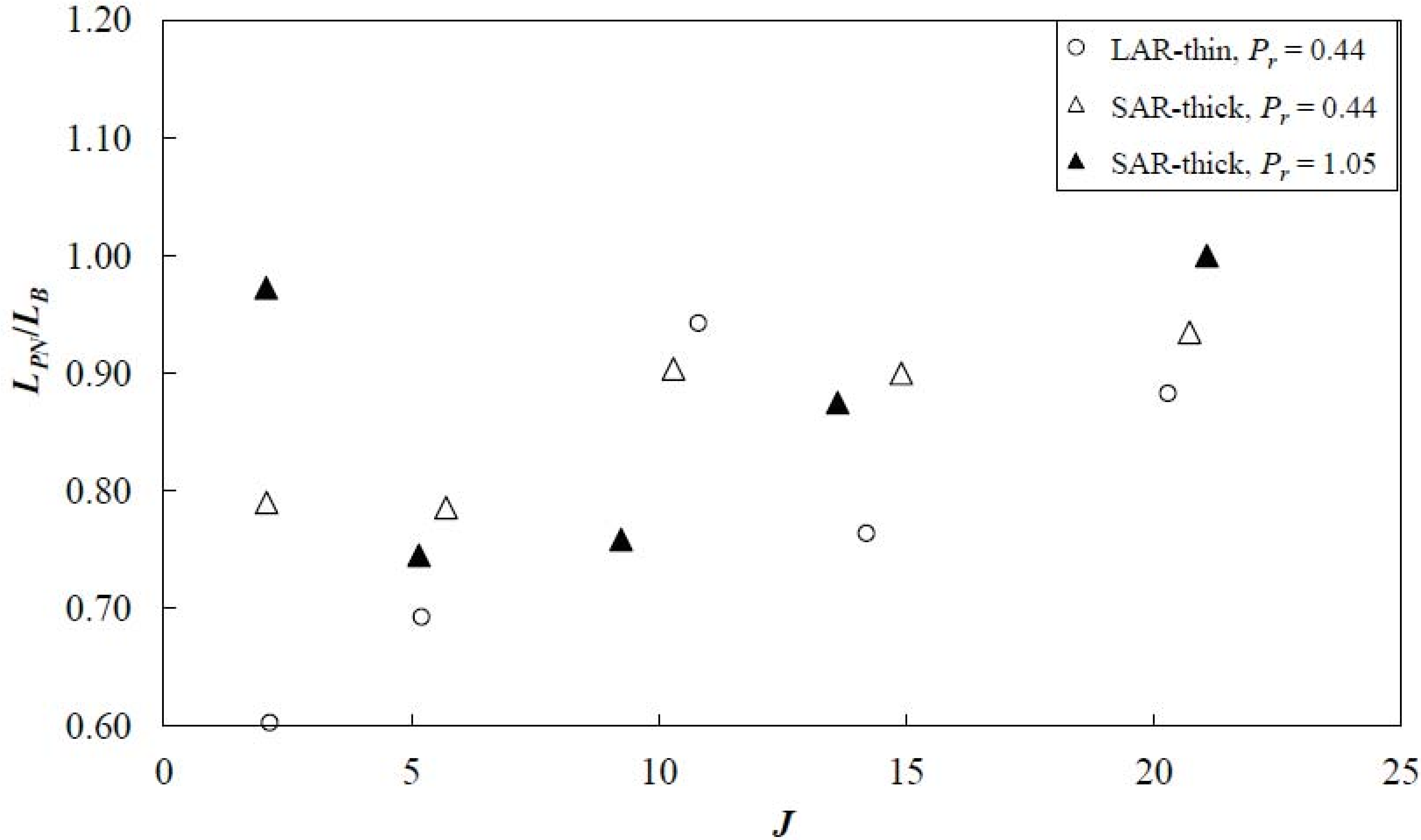

APPLICATION OF POD ON IMAGE PIXEL INTENSITIES

Proper Orthogonal Decomposition

• Proper Orthogonal Decomposition (POD) or Principal Component Analysis (PCA) was used for extracting dominant dynamical processes embedded in high-speed images.

• A time-resolved set of images $A(x,t)$ can be represented as a linear combination of orthonormal basis functions ϕ_k (aka proper orthogonal modes)[1,2] :

$$A(x,t) = \sum_{k=1}^{M} a_k(t)\phi_k(x)$$

where $a_k(t)$ are time dependent orthonormal amplitude coefficients and M is the number of modes

• Main idea: POD modal amplitudes capture the maximum possible “energy” in an average sense[3], i.e.,

$$\sum_k \langle a_k(t)a_k(t)\rangle \geq \sum_k \langle b_k(t)b_k(t)\rangle$$

where $b_k(t)$ are the temporal coefficients of a decomposition with respect to an arbitrary orthonormal basis ψ_k.

[1] **Chatterjee, A**. *Current Science*, Vol. 78, No. 7 (2000)
[2] **Arienti, M, and Soteriou, M.C.**. Phys. Fluids 21, 112104 (2009)
[3] **Berkooz, G., Holmes, P., and Lumley, J.L.**. *Annu. Rev. Fluid Mech.* 25. 539 (1993)

Construction of Data Set

- First, form a row vector consisting of all pixel intensity values of each snapshot image (with resolution of *n* rows by *m* columns) in order of increasing columns, then increasing rows

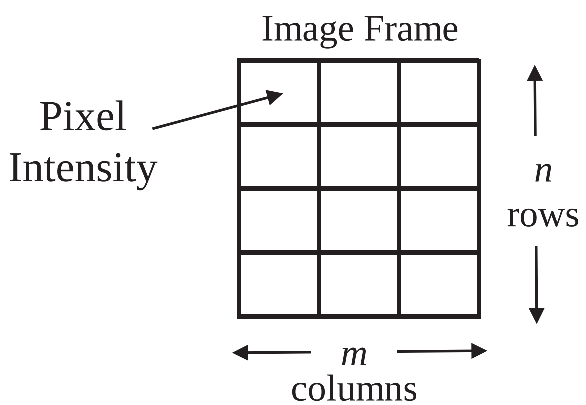

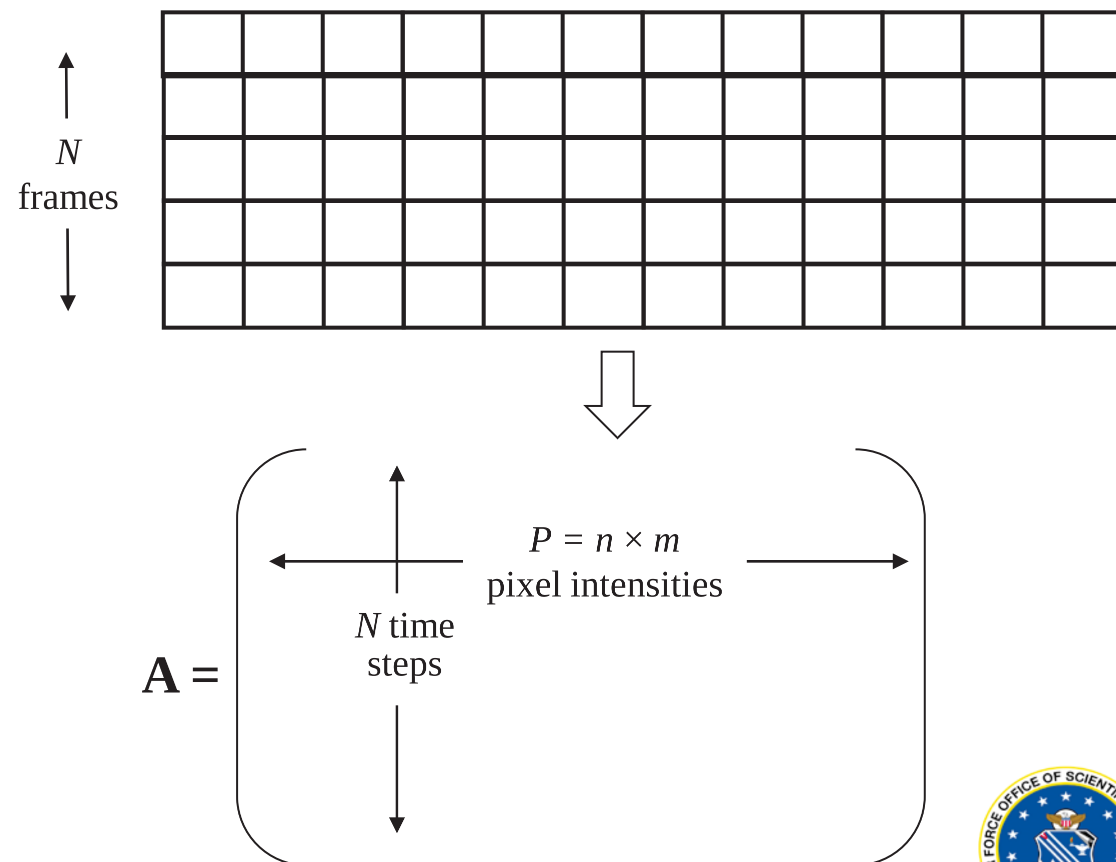

- Then, combine all such row vectors for N sequences of image frames resulting in a matrix **A** consisting of N rows by $P = n \times m$ columns of intensity values.

Orthogonal Decomposition Technique

- Eigenvalue decomposition or singular value decomposition (SVD) can be used
- SVD preferred since
  1. Applicable to non-square matrices (most likely the case)
  2. Decomposition matrices are orthogonal
  3. Subroutine readily available in MATLAB®
- Subtracted temporal mean of $\mathbf{A} \Rightarrow$ matrix of intensity fluctuations $\tilde{\mathbf{A}}$
- Applied SVD

$$\Rightarrow \tilde{\mathbf{A}} = \mathbf{USV}^{\mathrm{T}} = \mathbf{QV}^{\mathrm{T}}$$

Columns of $\mathbf{Q} \sim a_k(t)$ contain temporal information

Columns of $\mathbf{V} \sim \phi_k(x)$ contain spatial information

$\mathbf{U}$: $N \times N$
Orthogonal Matrix of Left Singular Column Vectors of $\tilde{\mathbf{A}}$

$\mathbf{V}$: $N \times P$
Orthogonal Matrix of Right Singular Column Vectors of $\tilde{\mathbf{A}} \Leftrightarrow$ proper orthogonal modes (POM)

$\mathbf{S}$: $N \times N$
Diagonal Matrix of Singular Values

Results – Baseline Low J Flow at P_r = 0.44

- LAR-thin , Pr = 0.44, J = 0.5

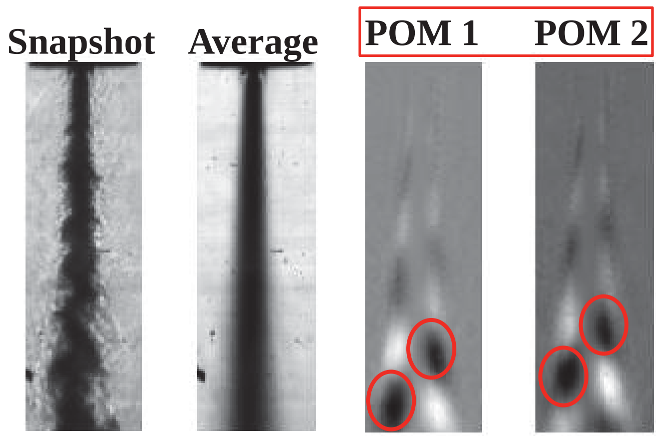

Amplitude information contained in singular values

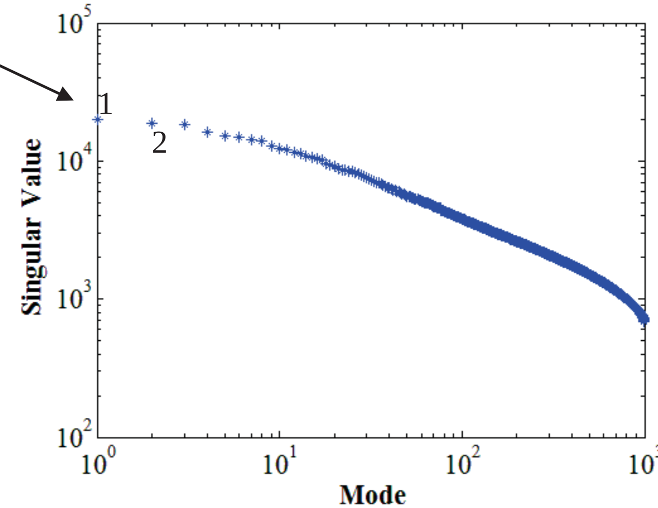

Antisymmetric Structures
Identified with Characteristic Frequencies

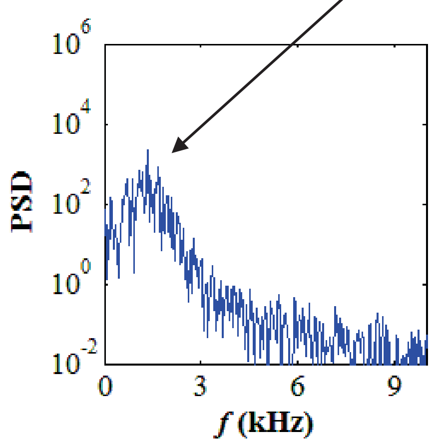

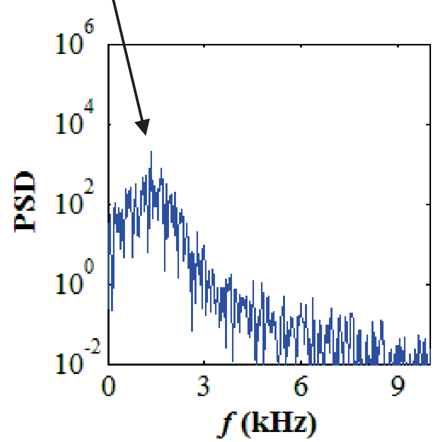

Power Spectral Densities (PSD) of Temporal Coefficients of POMs 1 and 2

Results – PAN Low J Flow at P_r = 0.44

- LAR-thin, Pr = 0.44, J = 0.5, forcing Frequency, f_F = 3.14 kHz

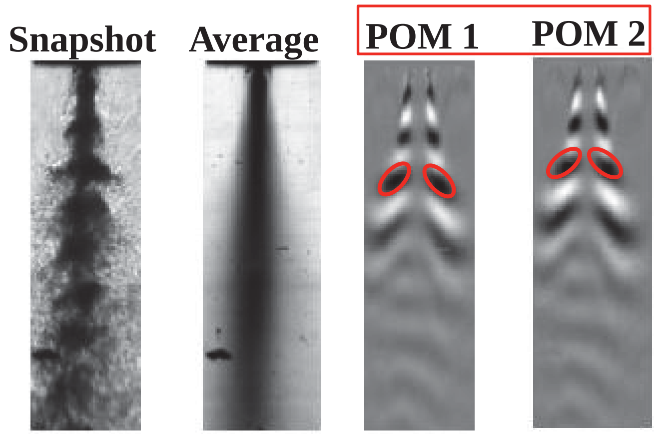

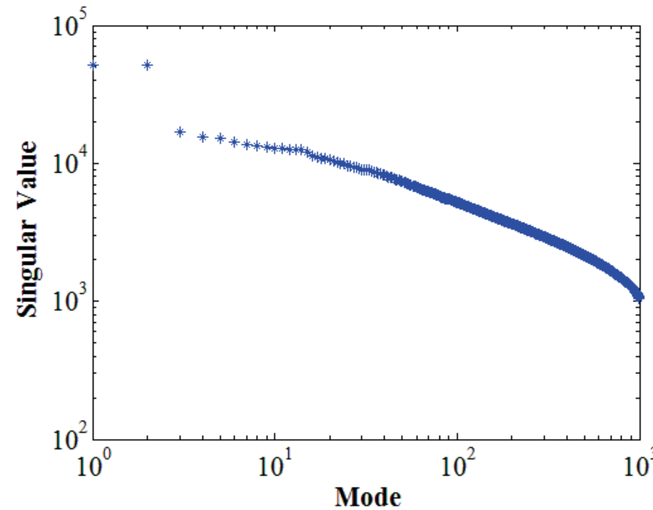

Symmetric Structures
Identified with Characteristic Frequency at f_F

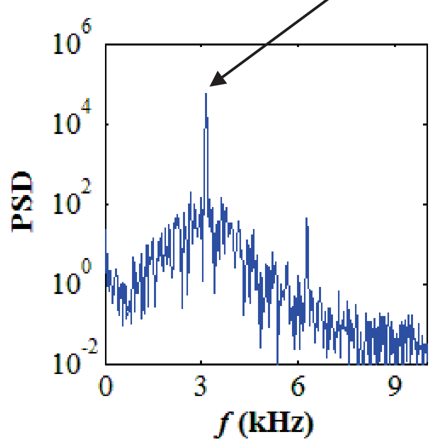

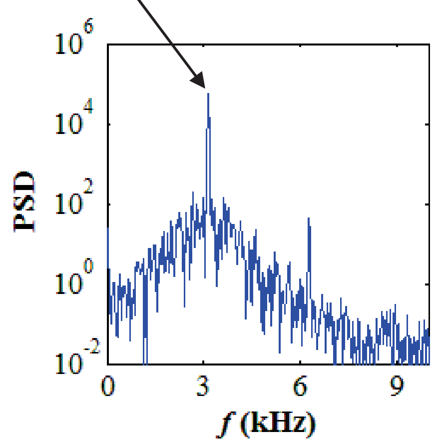

Results – PN Low *J* Flow at P_r = 0.44

- LAR-thin , *Pr* = 0.44, *J* = 0.5, forcing Frequency, f_F = 3.14 kHz

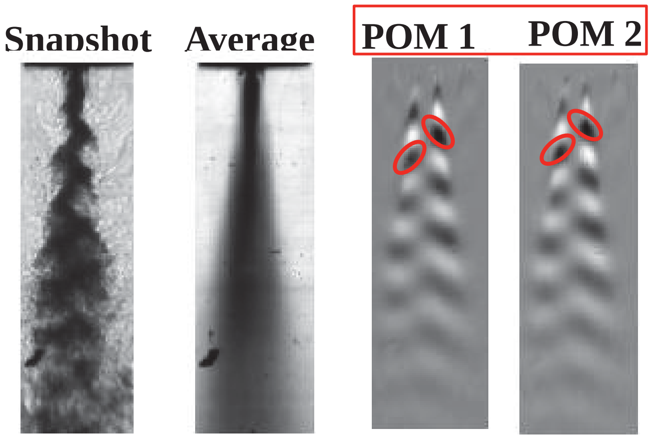

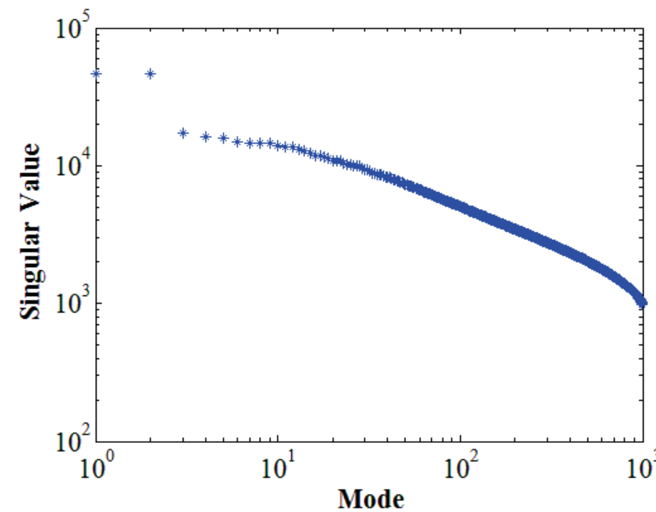

Antisymmetric Structures
Identified with Characteristic
Frequency at $\boldsymbol{f_F}$

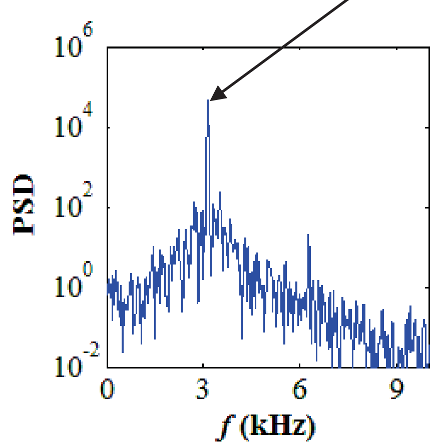

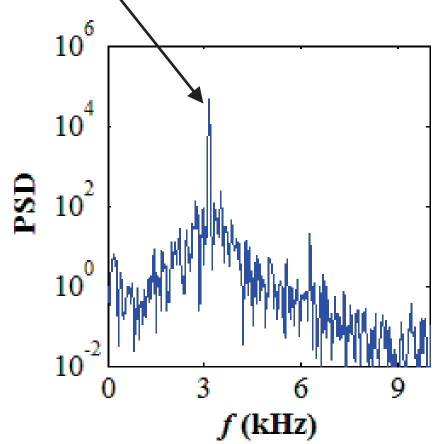

Cross-Power Spectral Density (CPSD)

- CPSD yields the FFT of the cross-correlation of the temporal coefficients

$$\mathrm{CPSD} = \sum_{k=0}^{N-1} \frac{\mathrm{cov}(a_x, a_y)}{\sigma_{a_x} \sigma_{a_y}} e^{-i\omega k}$$

- Magnitude and phase plots used to determine existence of propagating structures

<u>LAR, *Pr* = 0.44, *J* = 0.5</u>

Baseline

PAN (f_F = 3.14 kHz)

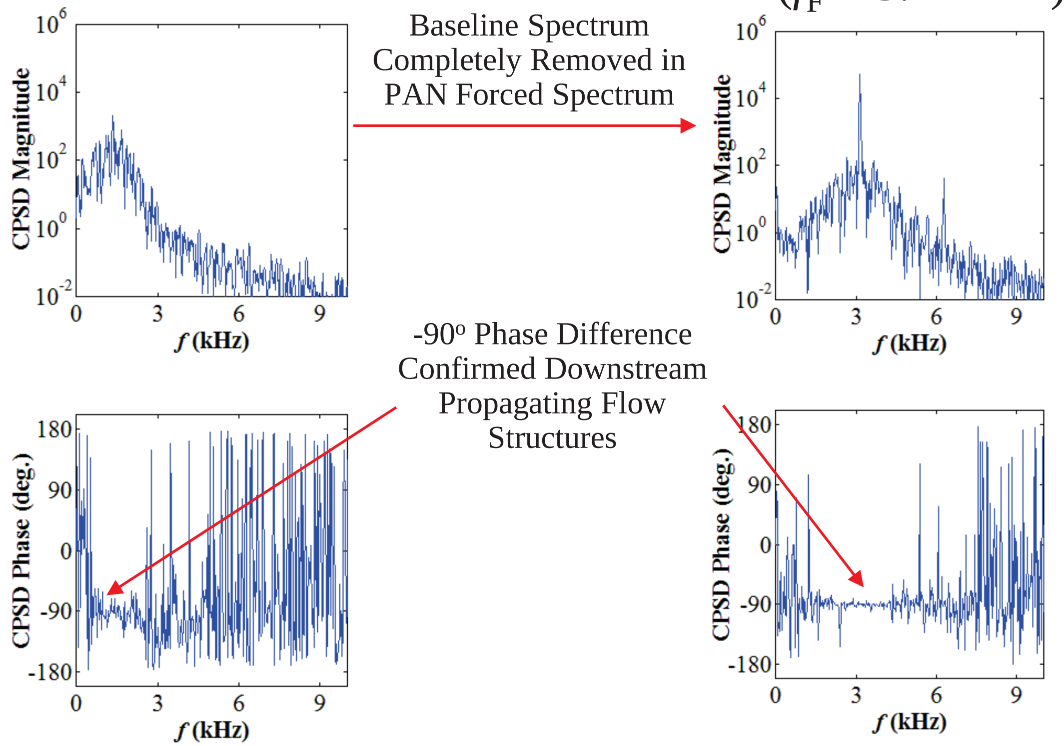

Sample Animation – PAN (f_F = 3.14 kHz)

- LAR Pr = 0.44, J = 0.5

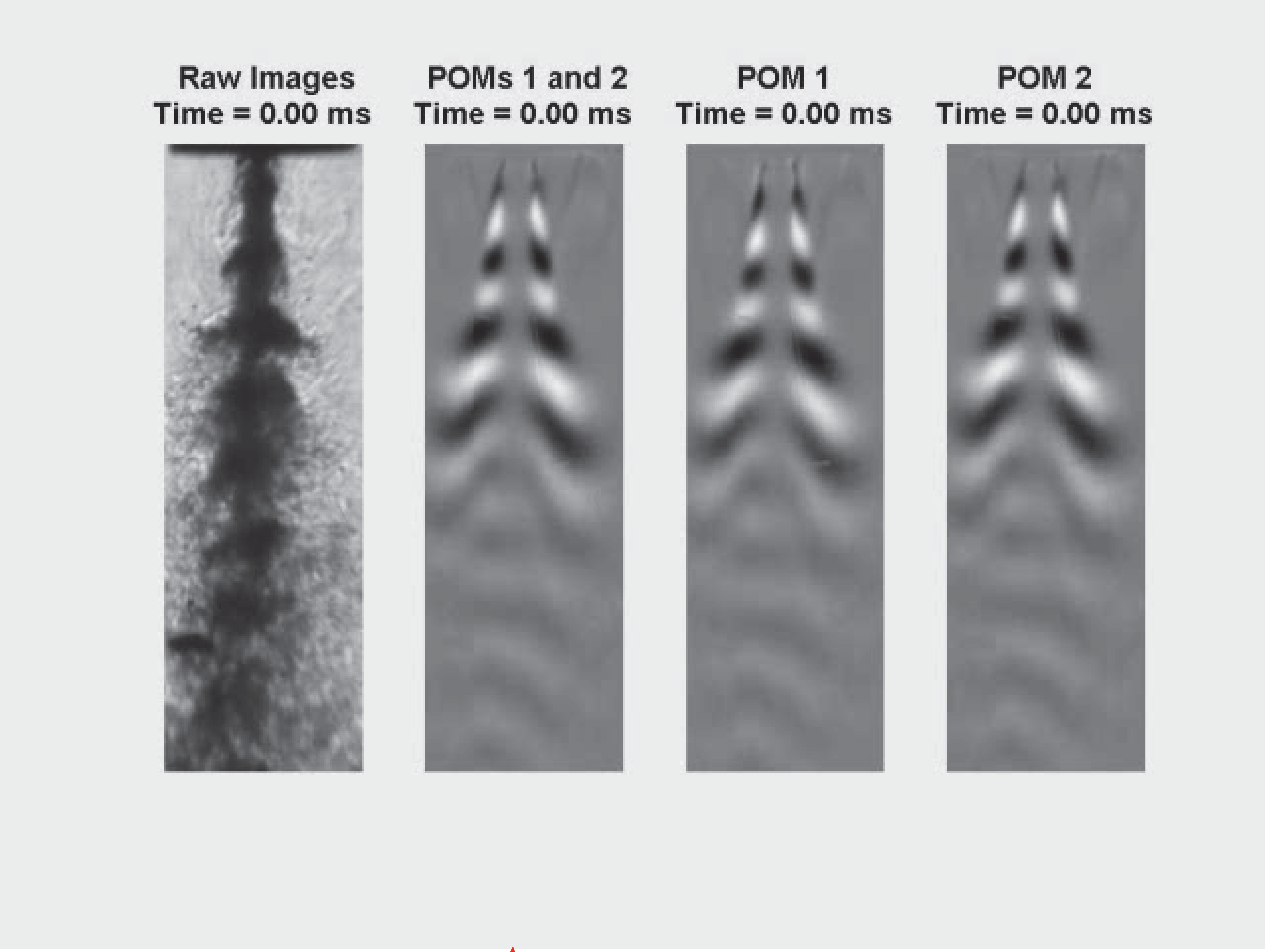

Superposition of POMs 1 and 2 Resulted in Downstream Propagating Structures

Baseline POM & CPSD: LAR-thin – P_r = 0.44

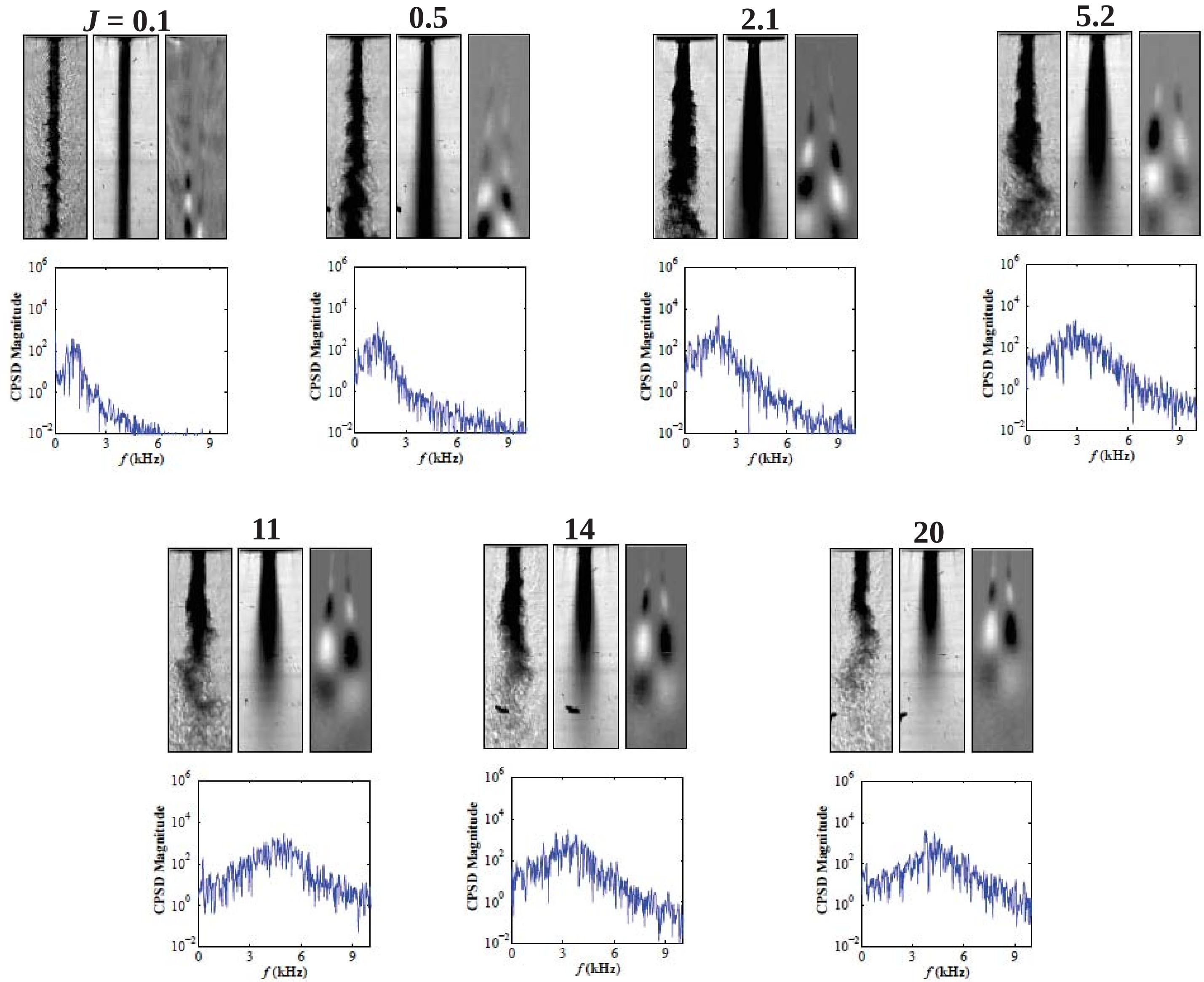

Baseline POM & CPSD: LAR-thin – $P_r = 1.05$

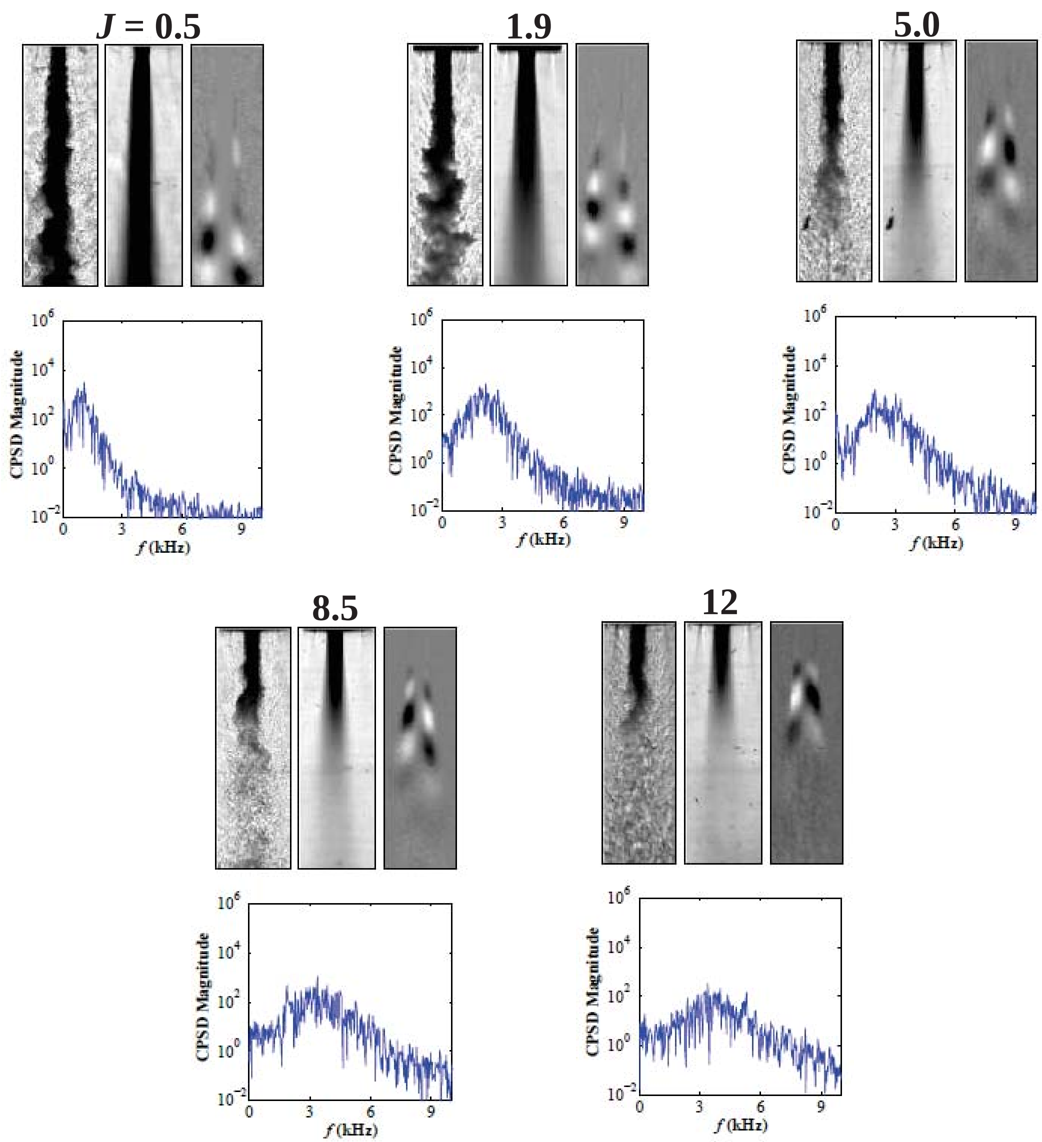

Previous Works on Jet Instability

- Michalke and Hermann (1982) did linear, inviscid instability analysis of a circular jet with coflow
- Showed that with increasing coflow velocity, U_∞
  - Helical disturbances more unstable than axisymmetric ones farther downstream of exit
  - Jet flow becomes less unstable, but spectrum of spatial growth rate becomes broader and the peak shifts to higher frequencies

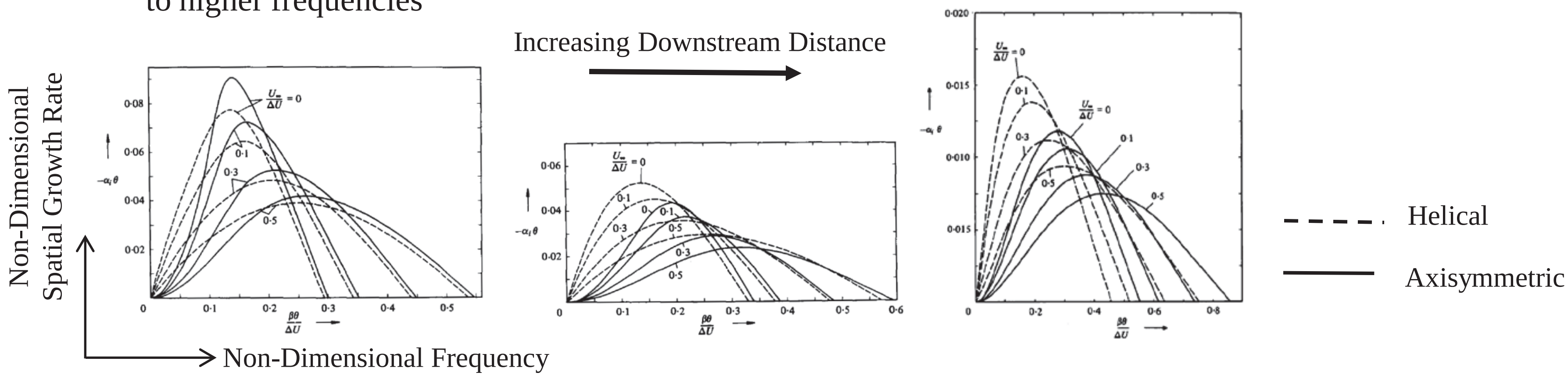

- Dahm *et al.* (1992), Wicker and Eaton (1994) conducted experimental investigation of large-scale vortex structures in the near field of coaxial jets
  - For outer-to-inner jet velocity ratios greater than one, found that coherent structures in the outer shear layer dominate those in the inner shear layer
  - At large axial distances, shear-layer vortices exhibit helical structures

Dahm *et al.*, *JFM* 1992

Baseline POM & CPSD: SAR-thick – $P_r = 0.44$

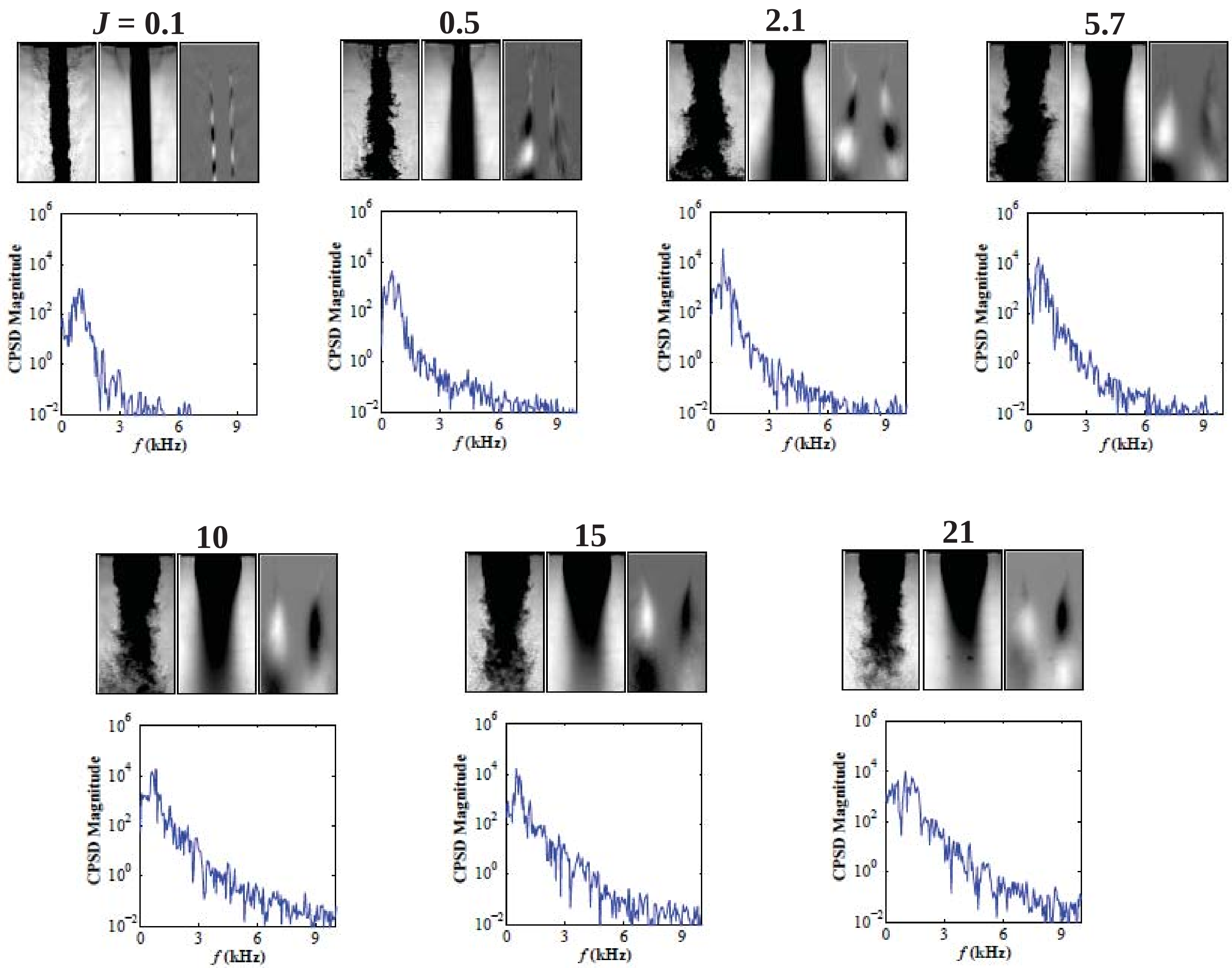

Baseline POM & CPSD: SAR-thick – P_r = 1.05

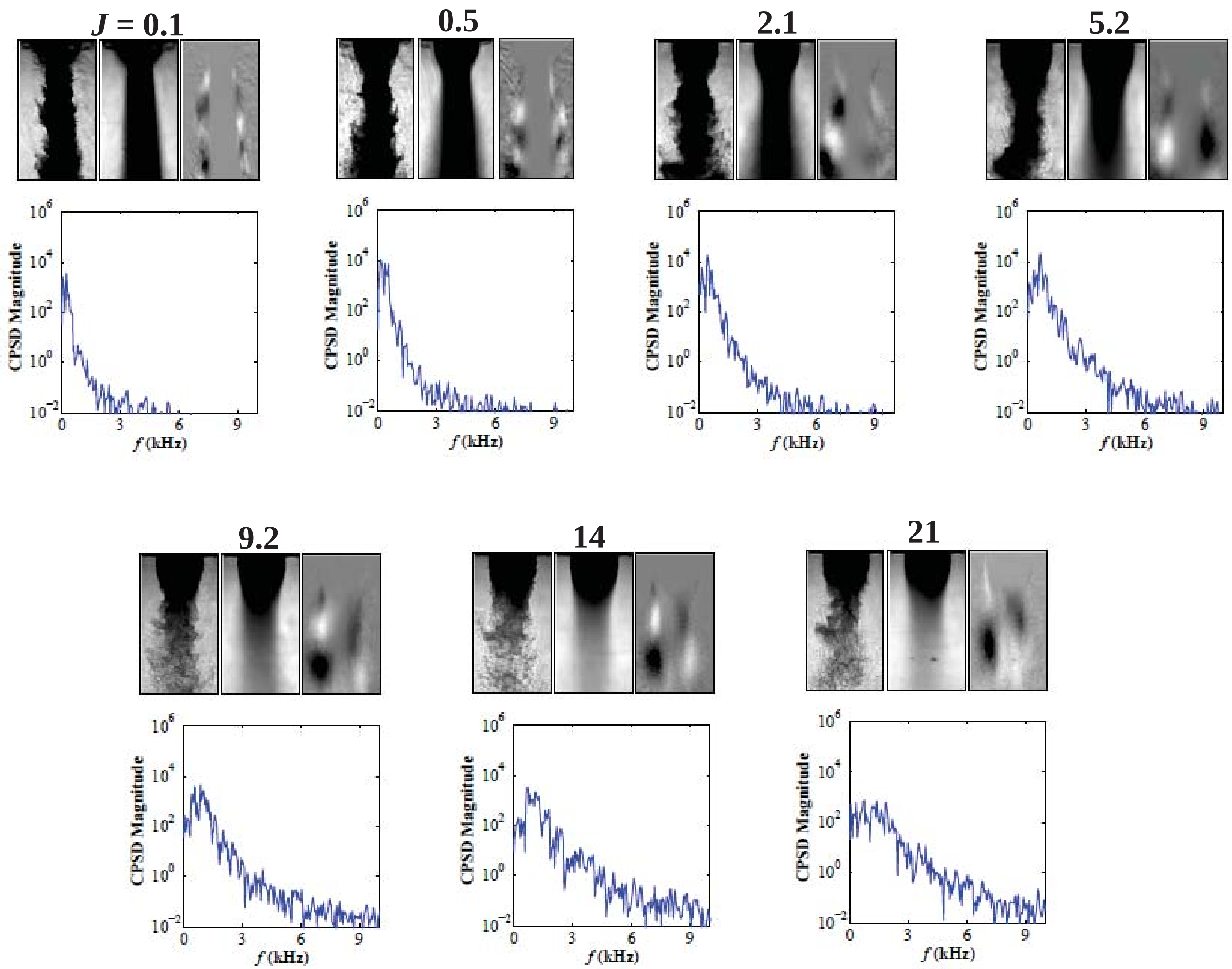

Inner Shear-Layer Structure Velocity – Pr = 0.44

LAR-thin

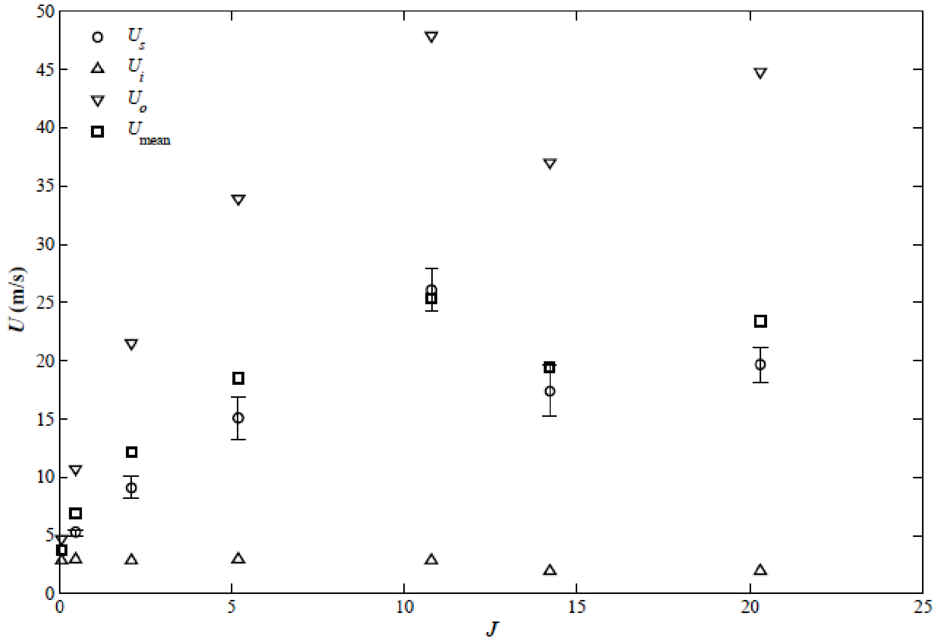

SAR-thick

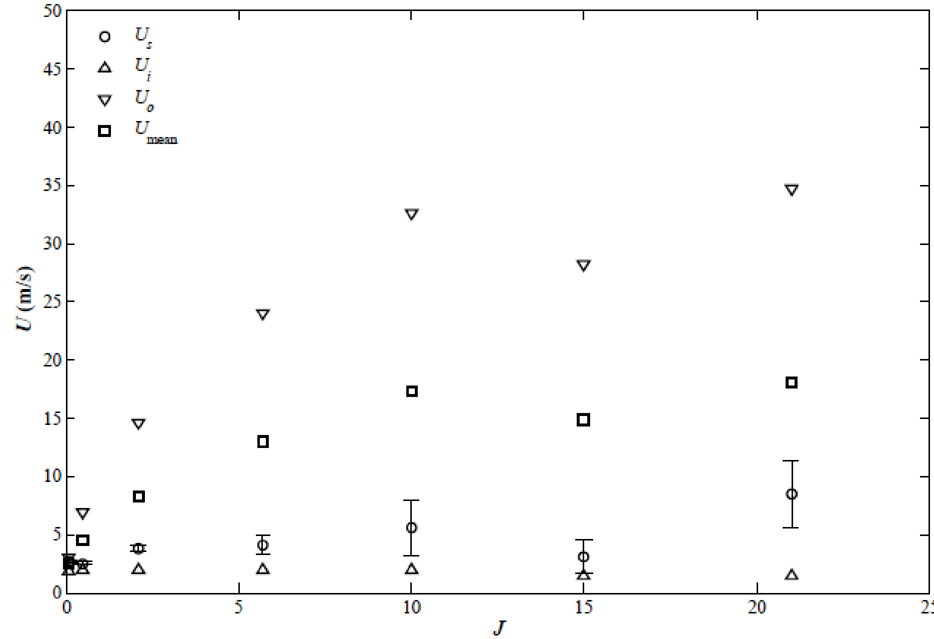

Inner Shear-Layer Structure Velocity – Pr = 1.05

LAR-thin

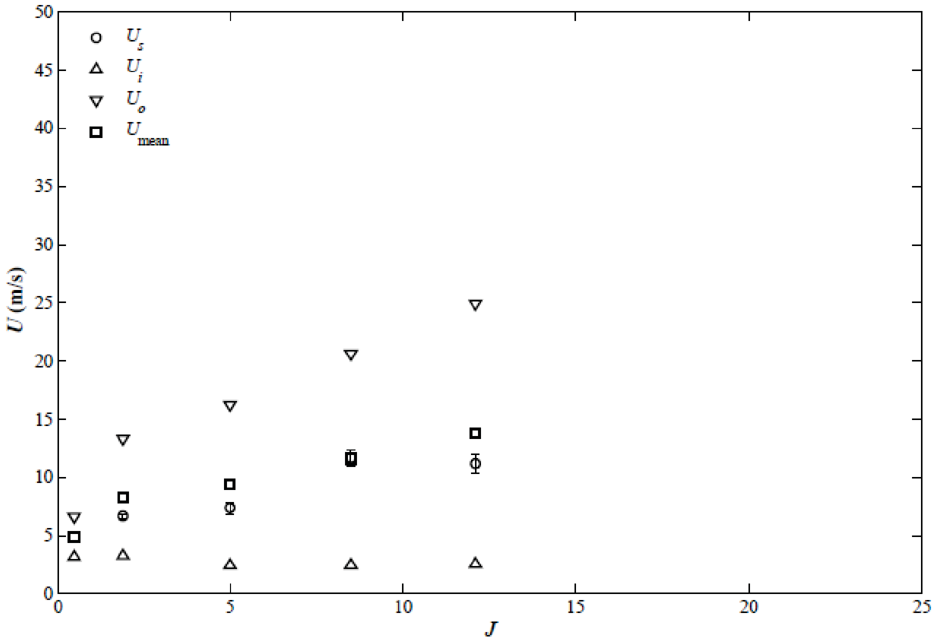

SAR-thick

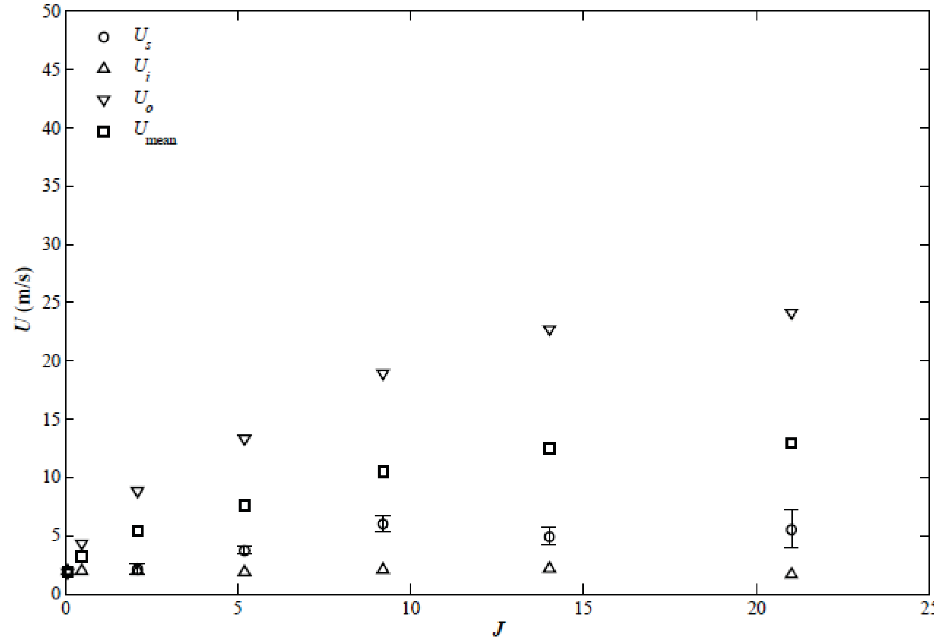

Forced POM & CPSD: LAR-thin – $P_r = 0.44$

$J = 0.1$

PAN

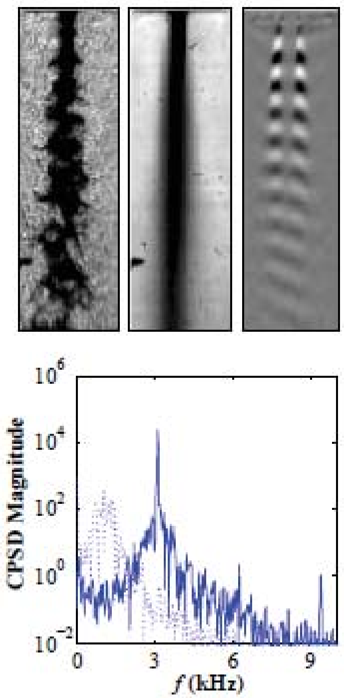

PN

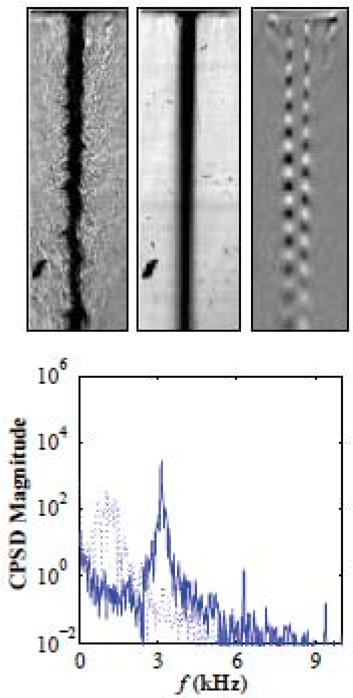

$J = 0.5$

PAN

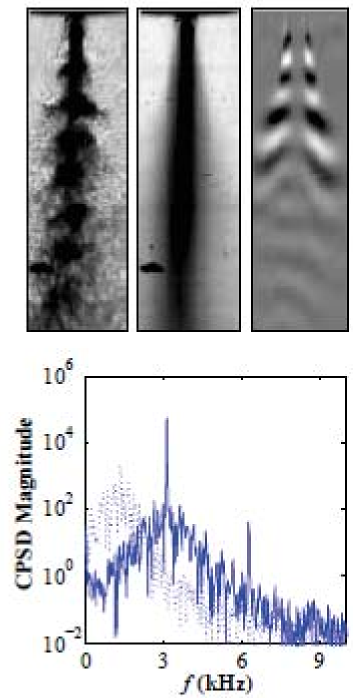

PN

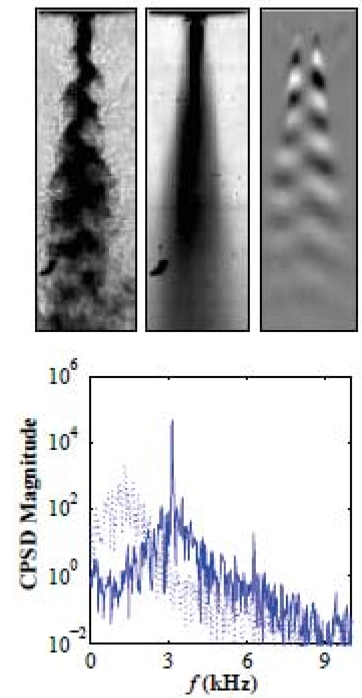

Forced POM & CPSD: LAR-thin – P_r = 0.44

<u>*J* = 2.1</u>

PAN

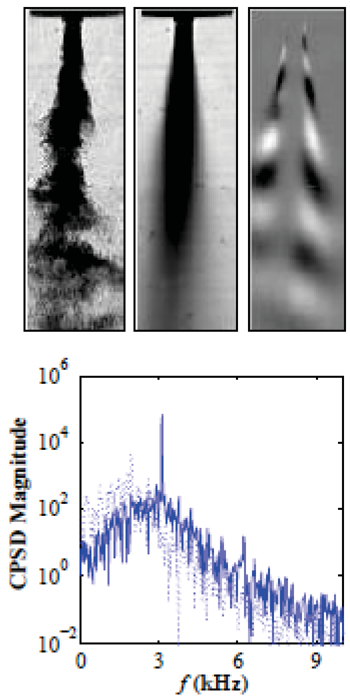

PN

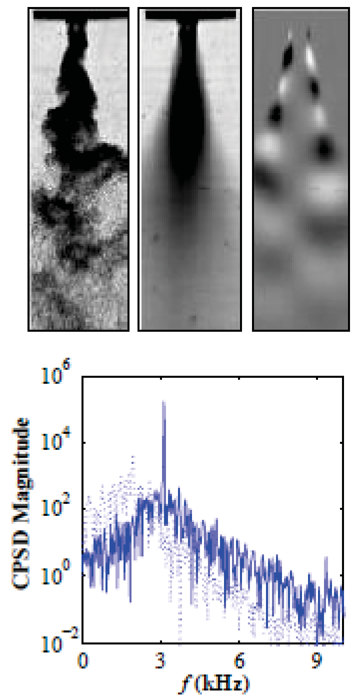

<u>*J* = 5.2</u>

PAN

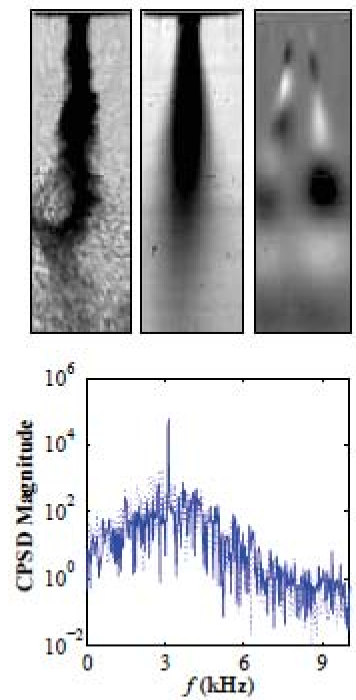

PN

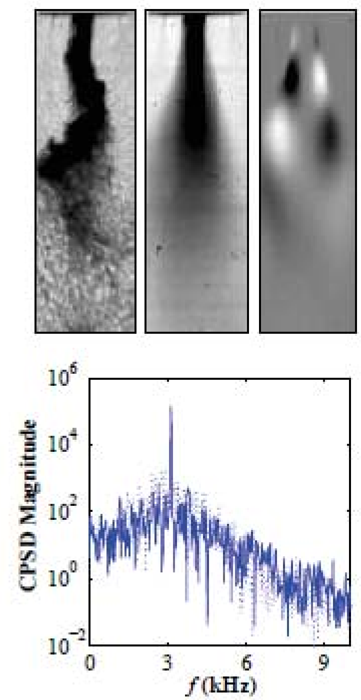

Forced POM & CPSD: LAR-thin – P_r = 0.44

<u>***J* = 11**</u>

PAN

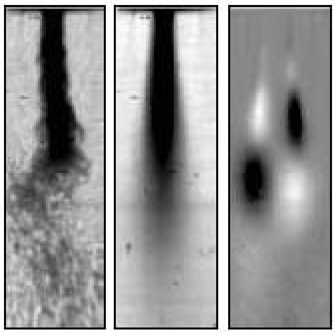

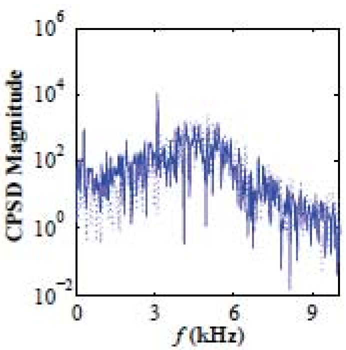

PN

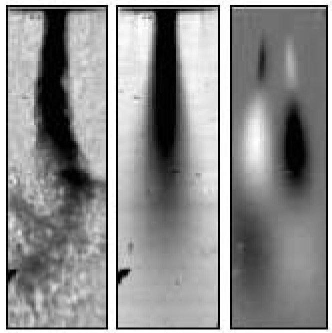

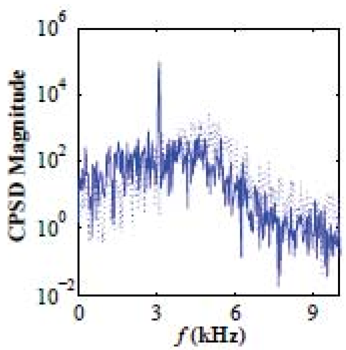

<u>***J* = 20**</u>

PAN

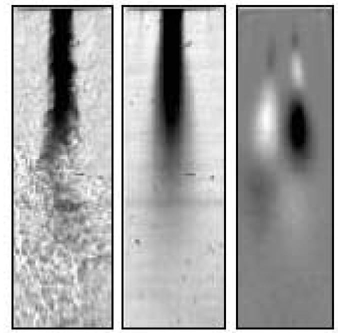

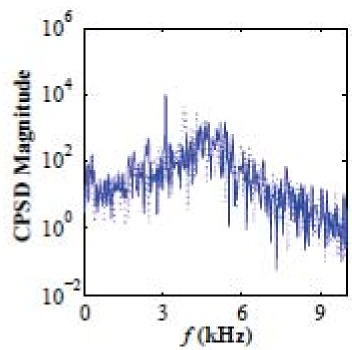

PN

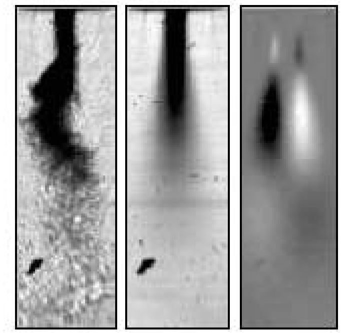

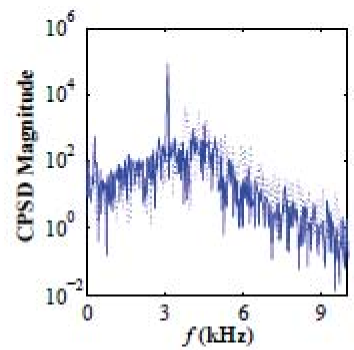

Forced POM & CPSD: LAR-thin – $P_r = 1.05$

$J = 0.5$

PAN

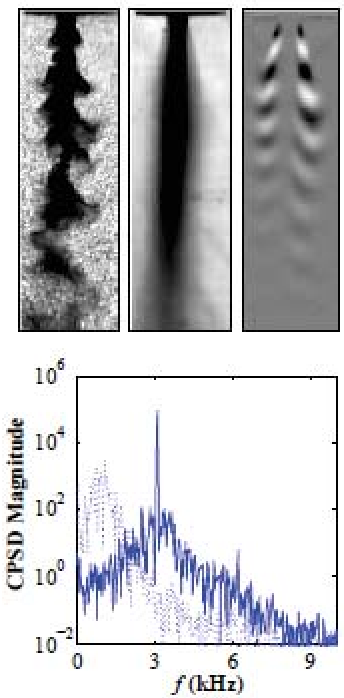

PN

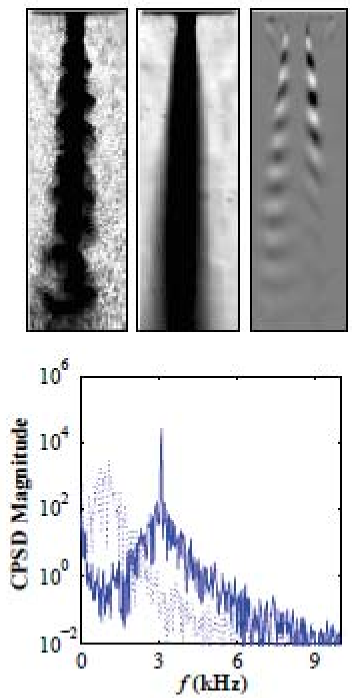

$J = 5.0$

PAN

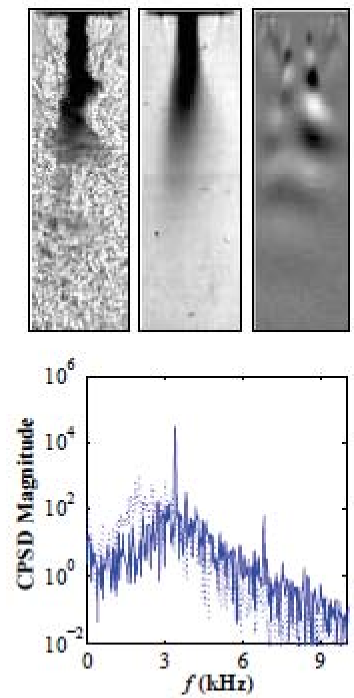

PN

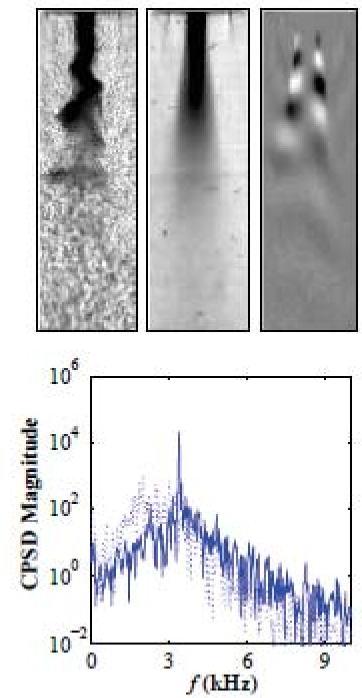

Forced POM & CPSD: LAR-thin – P_r = 1.05

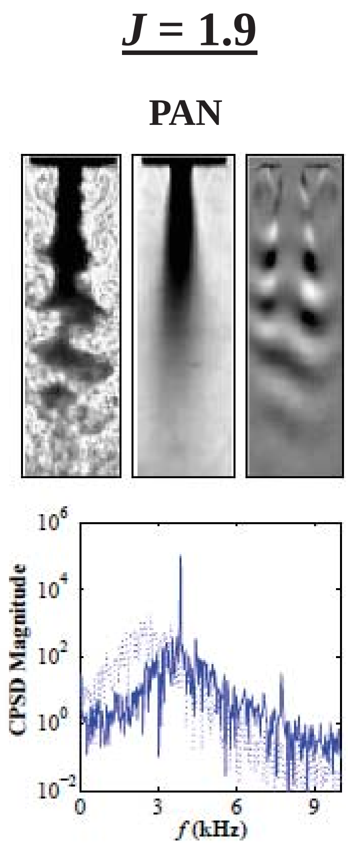

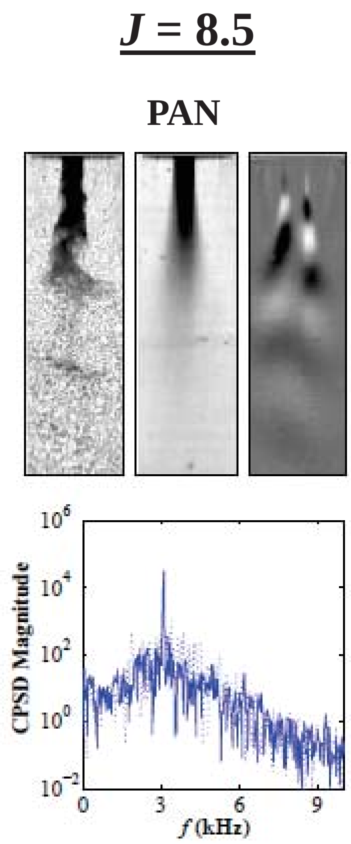

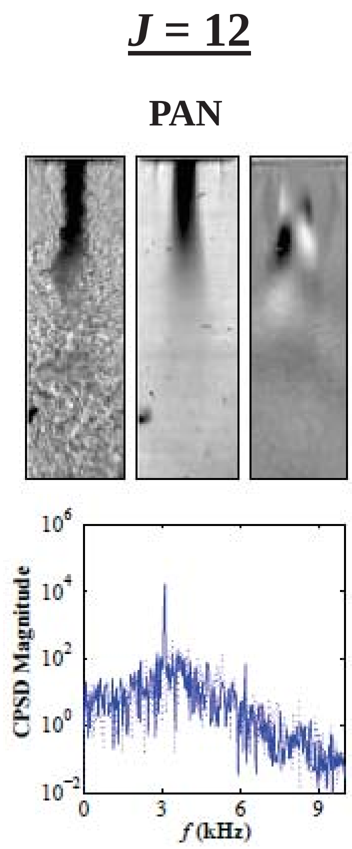

Forced POM & CPSD: SAR-thick – P_r = 0.44

<u>***J* = 0.1**</u>

PAN

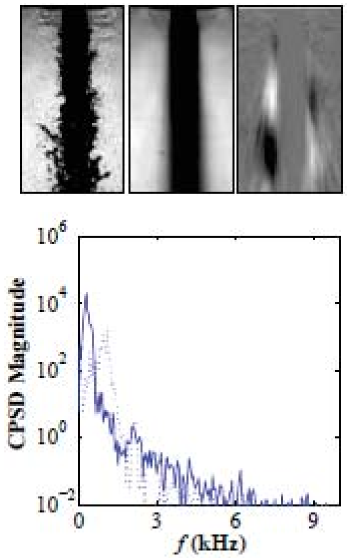

<u>***J* = 0.5**</u>

PAN

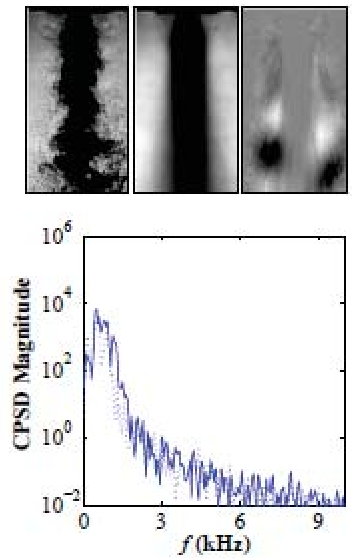

Forced POM & CPSD: SAR-thick – P_r = 0.44

***J* = 2.1**

PAN

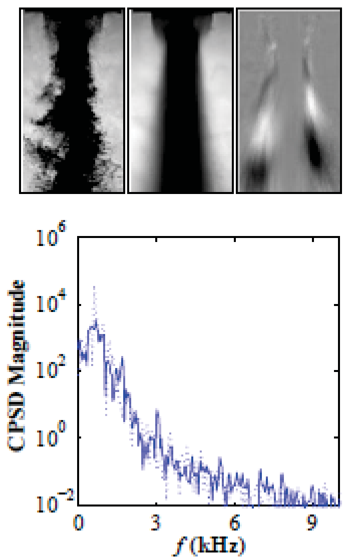

PN

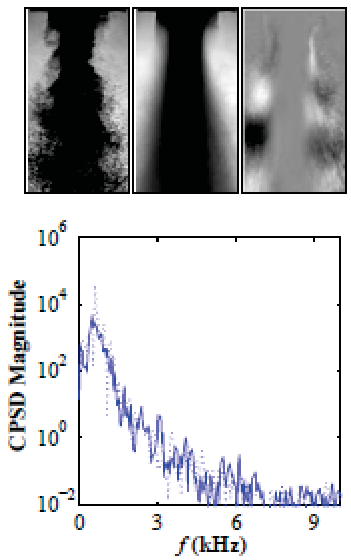

***J* = 5.7**

PAN

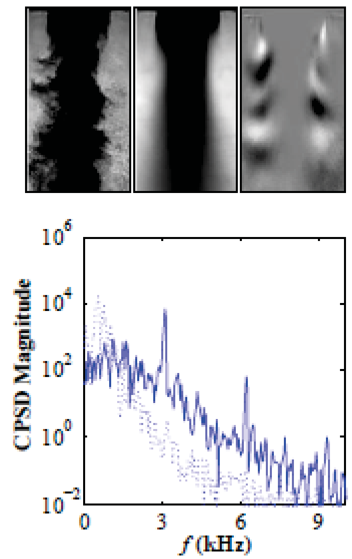

PN

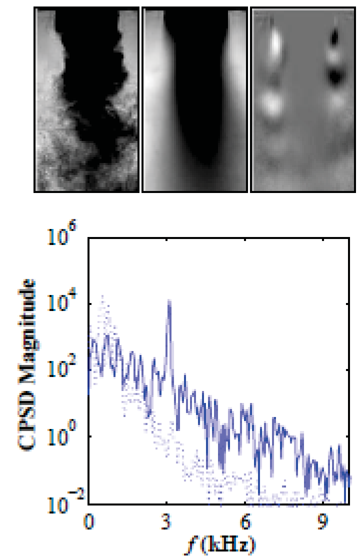

Forced POM & CPSD: SAR-thick – $P_r = 0.44$

$J = 10$

PAN

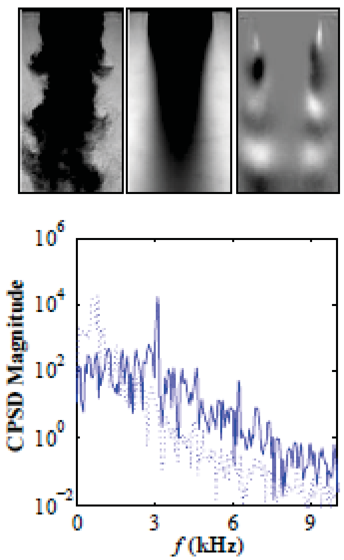

PN

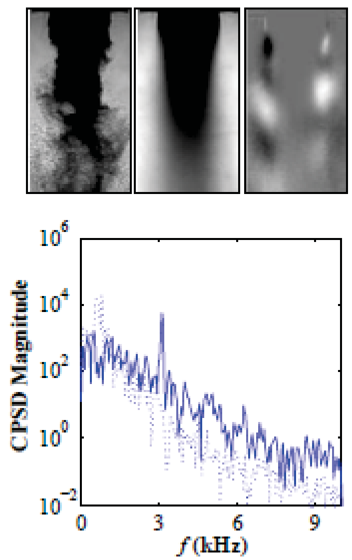

$J = 21$

PAN

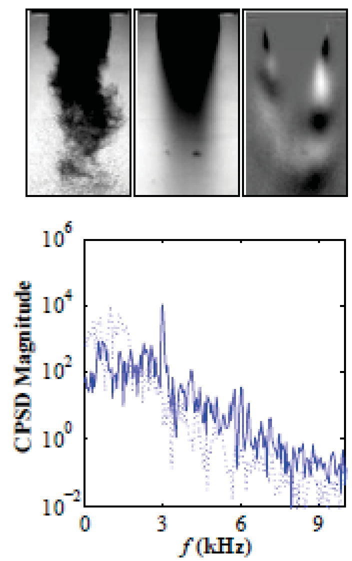

PN

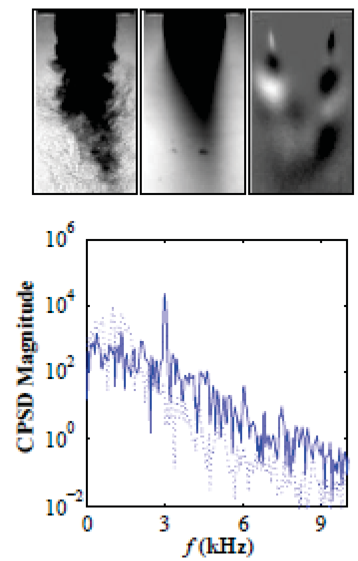

Forced POM & CPSD: SAR-thick – $P_r = 1.05$

$J = 0.5$

PAN

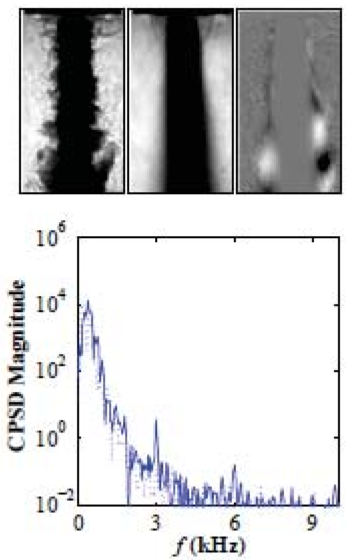

PN

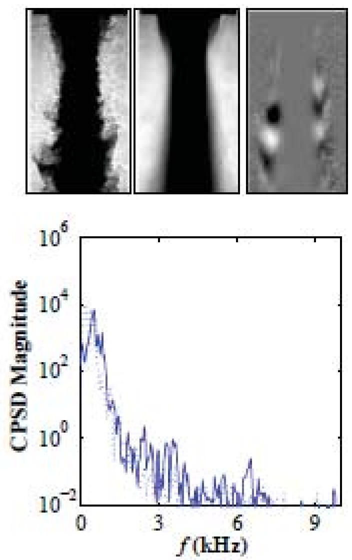

$J = 2.1$

PAN

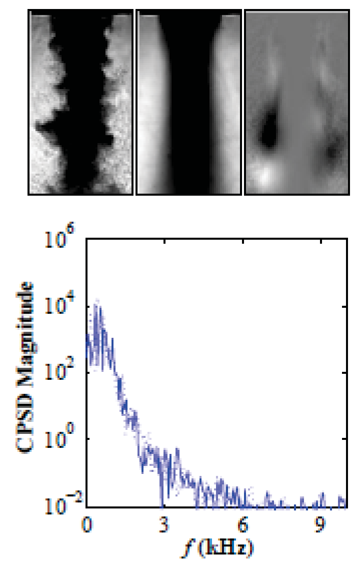

(a) $J = 2.1$, PAN

PN

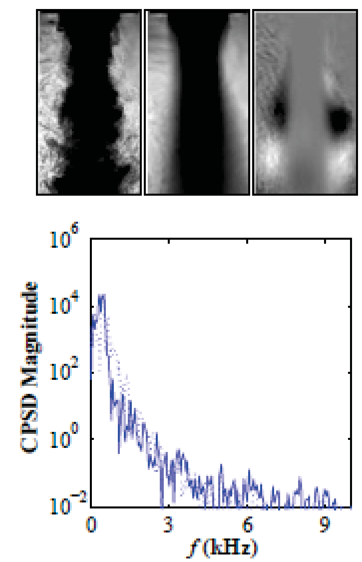

(b) $J = 2.1$, PN

Forced POM & CPSD: SAR-thick – P_r = 1.05

J = 5.2

PAN

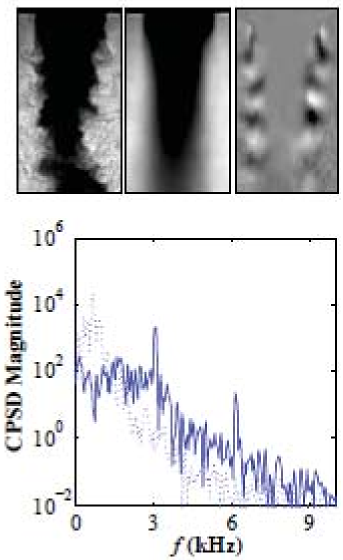

PN

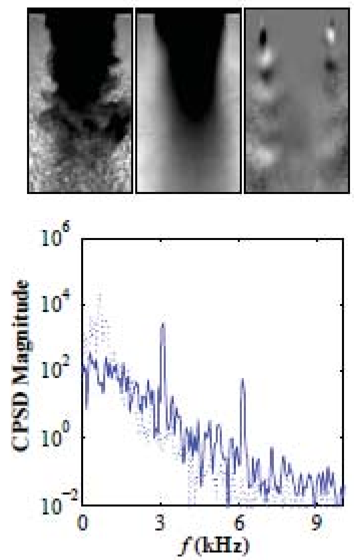

J = 9.2

PAN

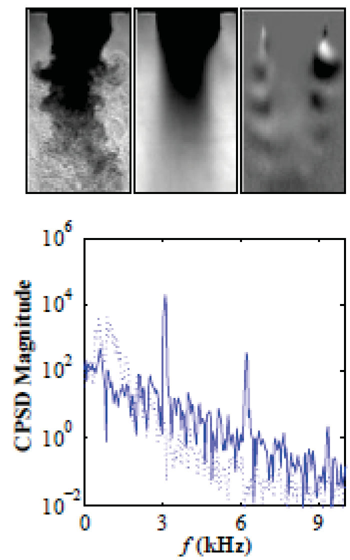

PN

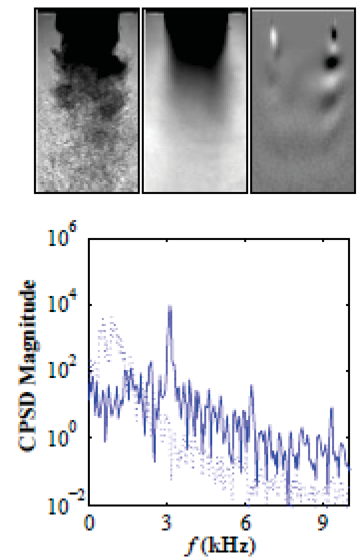

Forced POM & CPSD: SAR-thick – $P_r = 1.05$

$J = 14$

PAN

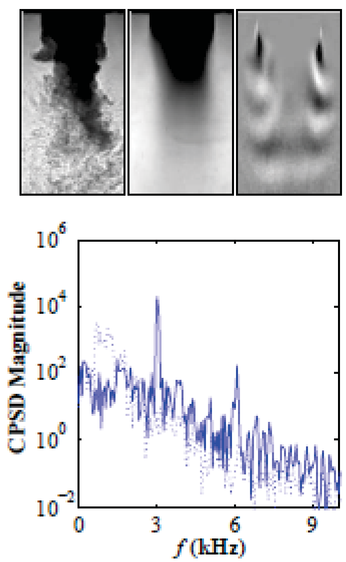

PN

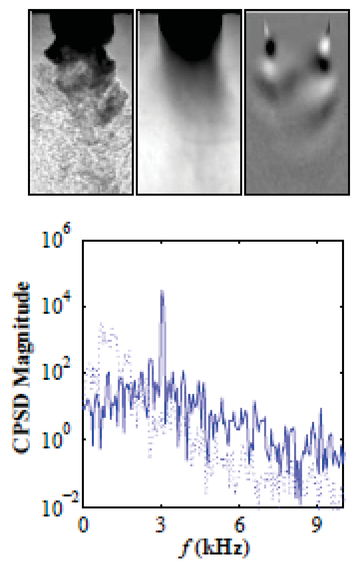

$J = 21$

PAN

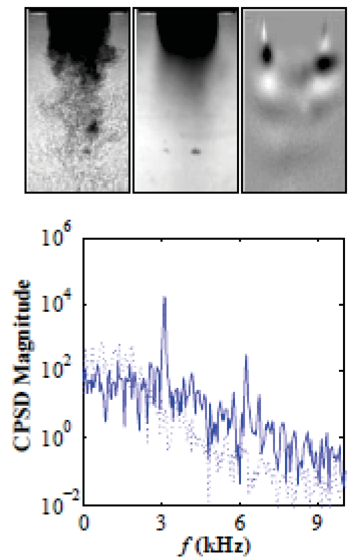

PN

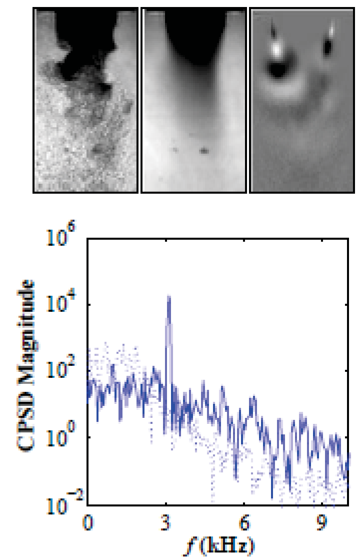

Conclusions

- Baseline flow normalized dark-core lengths, L_B/D_1:
  - Power-law curve-fit of L_B/D_1 variation with J showed that P_r = 1.05 cases had a stronger dependence ($J^{-0.50}$ for the LAR-thin and $J^{0.54}$ for the SAR-thick); P_r = 0.44 cases varied as $J^{-0.39}$ for the LAR-thin and $J^{-0.35}$ for the SAR-thick.
  - For a given J and same P_r, SAR-thick flows had smaller L_B/D_1 than LAR-thin flows
  - Considering the LAR-thick and SAR-thin injector flow data at both P_r, it can be deduced that L_B/D_1increased with A_o/A_i while it decreased with J and t/D_1

    $\Rightarrow$ injector geometry also plays an important role in addition to J

- Acoustically forced flow normalized dark-core lengths, $L_{PAN/}/L_B$ or $L_{PN/}/L_B$:
  - LAR-thin injector
    - Both $L_{PAN/}/L_B$ and $L_{PN/}/L_B$ less than one and approached one with increasing J

    $\Rightarrow$ The flow became less sensitive to forcing with increasing J.
  - SAR-thick injector
    - For low J (< 10) flows, $L_{PAN/}/L_B$ stayed around one
    - $L_{PN/}/L_B$ approached one with increasing J

    $\Rightarrow$ Flow in recirculation zone only effective in dampening the effect of PAN forcing at lower J

Conclusions (cont'd)

- Dynamic characteristics of baseline flows:
  - LAR-thin injector:
    - inner shear layer formed immediately downstream of the exit
    - baseline flow inner shear layer characterized by antisymmetric flow structures that indicated the presence of helical instabilities
    - peak frequencies of the magnitude spectra became broader and shifted to higher frequencies with increasing J
  - SAR-thick injector:
    - region immediately downstream of the thick inner jet post formed a flow recirculation zone delaying formation of shear layer between the bulk inner and outer jets
    - peak frequencies stayed at low frequencies despite increasing J

Conclusions (cont'd)

- Dynamic characteristics of forced flows:
  - LAR-thin injector:
    - PAN forcing produced symmetric flow structures in the inner shear layer region for low J (< 5) flows at both P_r
    - Magnitude spectra showed dominant peaks identical to the forcing frequency
    - Higher J (> 5) flows under PAN forcing produced antisymmetric structures that resembled that of baseline
    - Magnitude spectra retained baseline flow spectral characteristics
    - peak frequencies of the magnitude spectra became broader and shifted to higher frequencies with increasing J
    - PN forcing produced sinusoid disturbance
  - SAR-thick injector:
    - PAN forcing produced no appreciable response in the inner shear layer of the low J (< 5) flows, at both P_r
    - Spectra showed low frequency peaks, and no peaks at forcing frequencies were detected
    - at higher J (>5) and both Pr, PAN forcing produced symmetric structures below the recirculation zone with peaks in the spectra at the forcing frequencies
    - PN forcing also produced appreciable response at higher J

Acknowledgement

- Technicians
  - Randy Harvey, David Hill, Earl Thomas (ERC)
  - Todd Newkirk (Jacobs Engineering)
- SAR Data
  - Dr. Juan Rodriguez
- This work is sponsored by the Air Force Office of Scientific Research under Dr. Mitat Birkan, program manager.

Back-Up Slides

Acoustic Field Set-Up: Pressure Node

- Pressure node (PN) – condition of minimum pressure perturbation in the acoustic field
- Piezo-sirens forced out-of-phase
- Superposition of quasi-1D acoustic waves traveling in opposite directions ⇒ PN at the jet location (geometric center of test section)

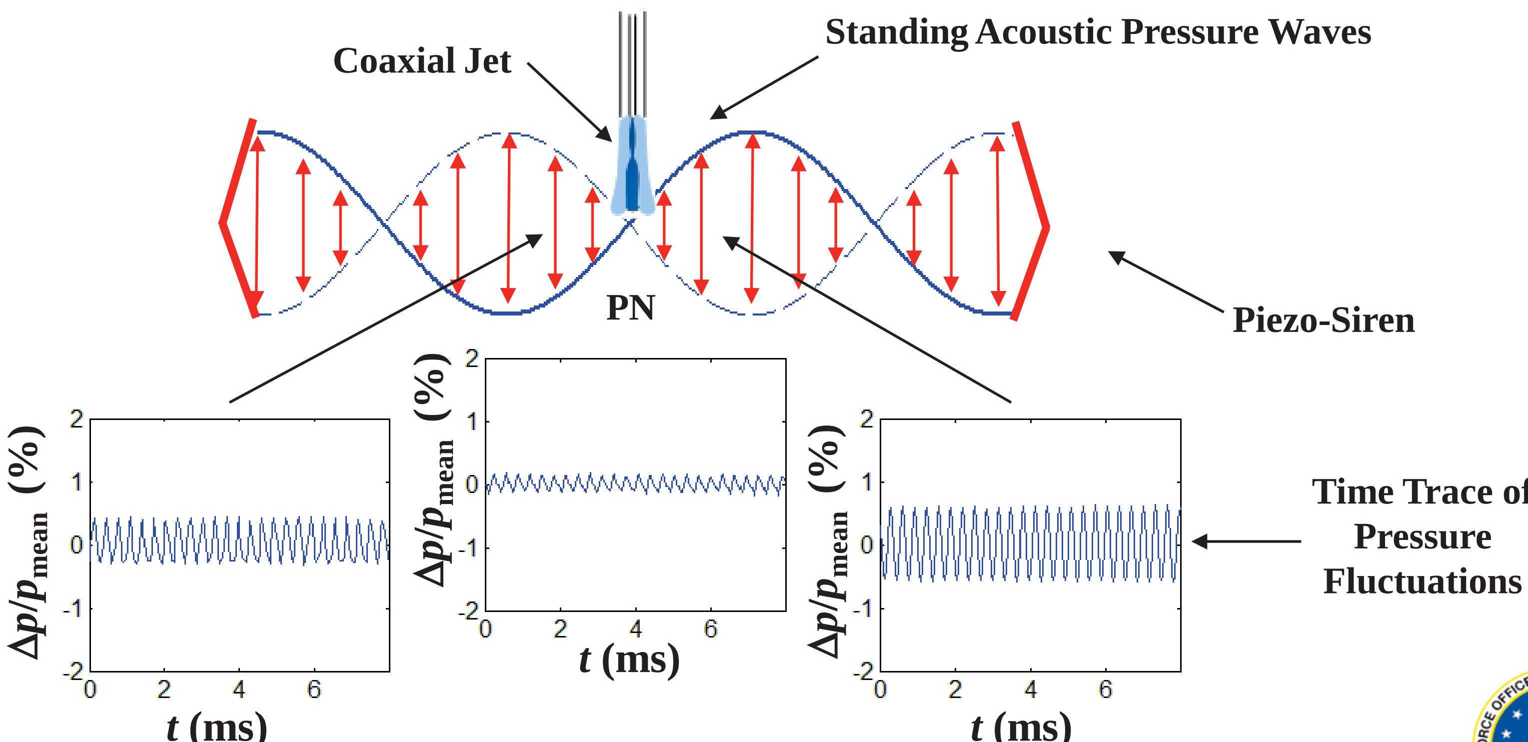

Baseline Normalized DCL, L_B/D_1 – LAR-thin

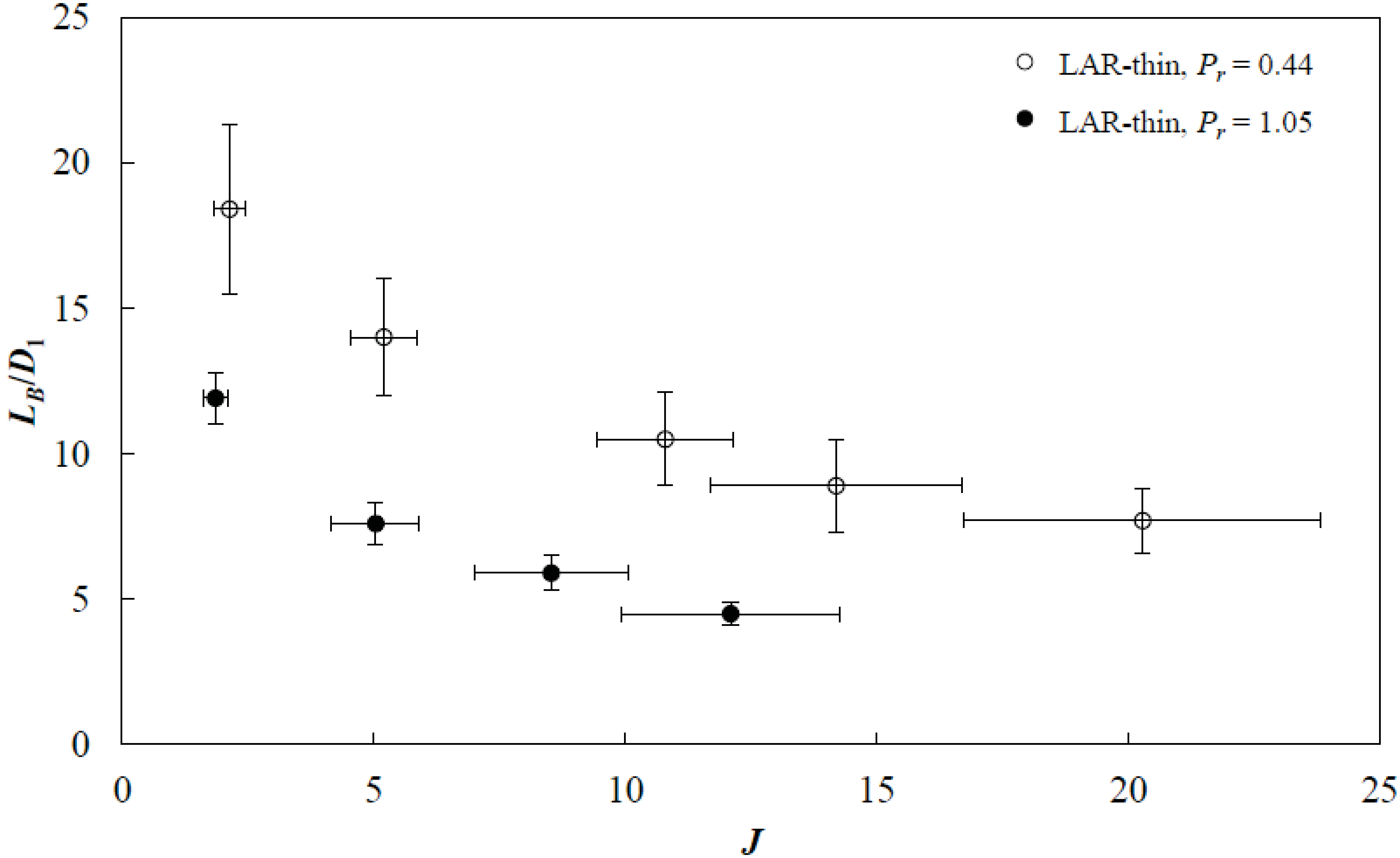

Baseline Normalized DCL, L_B/D_1 – SAR-thick

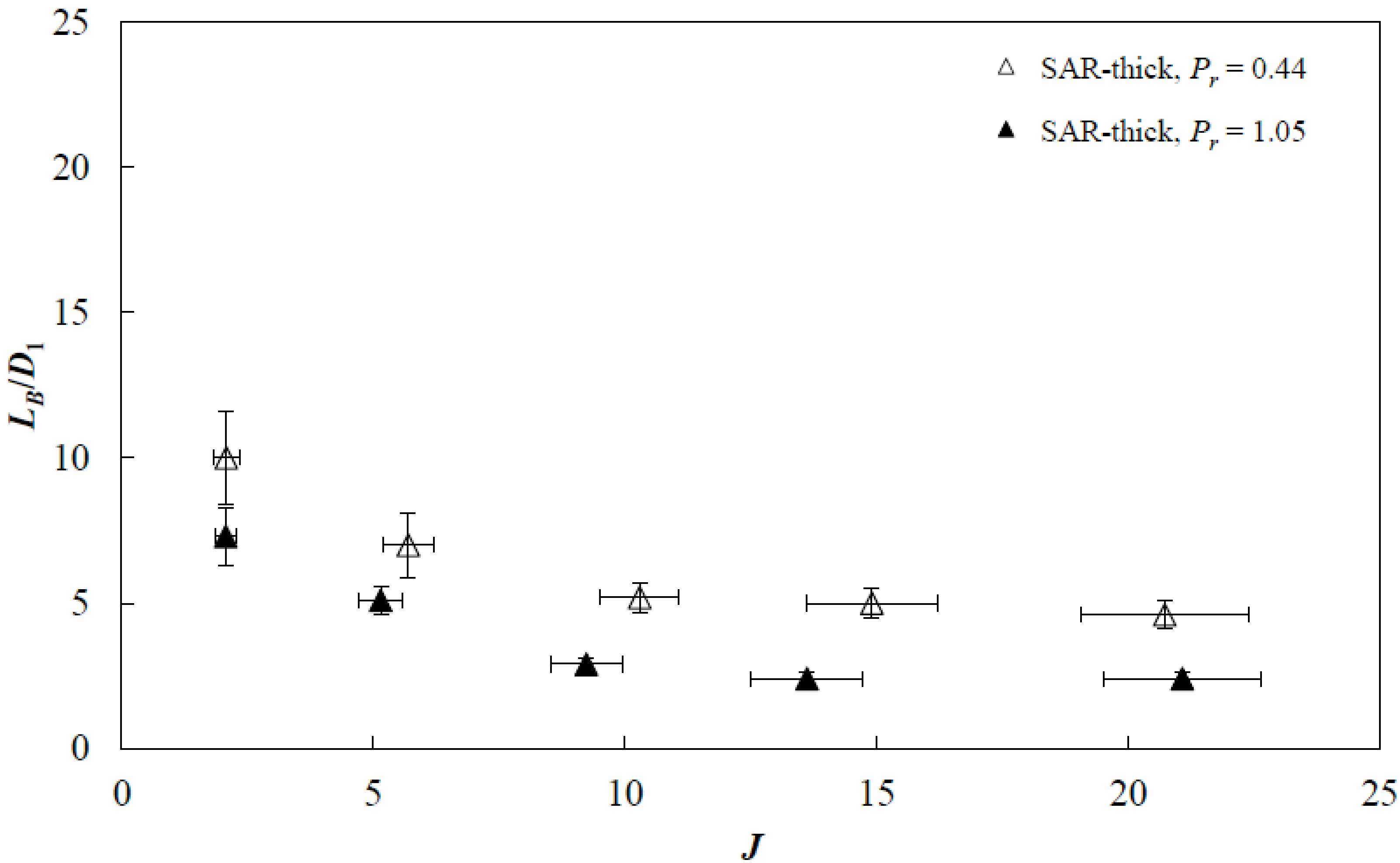

Distribution A: Approved for Public Release; Distribution Unlimited